Autophagosomes fuse to phagosomes and facilitate the degradation of apoptotic cells in *Caenorhabditis elegans*

Omar Peña-Ramos[1], Lucia Chiao[1], Xianghua Liu[1,2], Tianyou Yao[1], Henry He[1,3], and Zheng Zhou[1,4]

[1] Verna and Marrs McLean Department of Biochemistry and Molecular Biology, Baylor College of Medicine, Houston, TX 77030

[2] Current address: Caris Life Sciences, Inc., Tempe, AZ 85281

[3] Current address: Department of Neurology Residency Program, University of Texas Southwestern Medical Center, Dallas, TX 75390

[4] Corresponding author, zhengz@bcm.tmc.edu, 713-798-6489

Abstract

Autophagosomes are double-membrane intracellular vesicles that degrade protein aggregates, intracellular organelles, and other cellular components. During the embryonic development of the nematode *Caenorhabditis elegans*, 113 somatic cells undergo apoptosis. These cells are engulfed and degraded by their neighboring cells. We discovered a novel role of autophagosomes in facilitating the degradation of apoptotic cells in *C. elegans* embryos using a real-time imaging technique. Specifically, the double-membrane autophagosomes in engulfing cells are recruited to the surfaces of phagosomes containing apoptotic cells and subsequently fuse to phagosomes, allowing the inner vesicle to enter the phagosomal lumen. Mutants defective in the production of autophagosomes display significant defects in the degradation of apoptotic cells, demonstrating the important contribution of autophagosomes to this process. The signaling pathway led by the phagocytic receptor CED-1, the adaptor protein CED-6, and the large GTPase dynamin (DYN-1) promotes the recruitment of autophagosomes to phagosomes. Moreover, the subsequent fusion of autophagosomes with phagosomes requires the functions of the small GTPase RAB-7 and the HOPS complex components. Our findings reveal that, unlike the single-membrane, LC3-associated phagocytosis (LAP) vesicles reported for mammalian phagocytes, the canonical double-membrane autophagosomes facilitate the clearance of *C. elegans* apoptotic cells. These findings add autophagosomes to the collection of intracellular organelles that contribute to phagosome maturation, identify novel crosstalk between the autophagy and phagosome maturation pathways, and discover the upstream factors that initiate this crosstalk.

Introduction

During metazoan development and adulthood, a large number of cells undergo apoptosis or cell suicide; these dying cells are engulfed by phagocytes and degraded inside phagosomes, vacuoles composed of the lipid bilayers originated from the plasma membrane [1,2]. Swift engulfment and degradation of apoptotic cells are critical for tissue remodeling, the resolution of the wound area, and the prevention and suppression of harmful inflammatory and autoimmune responses induced by the contest of the dying cells [2]. Critical to the degradation of phagosomal contents is the fusion of intracellular organelles, including lysosomes and early endosomes, to phagosomes, which results in the delivery of the content of these organelles to the phagosomal lumen [3]. Lysosomes, which contribute many kinds of hydrolytic enzymes, including proteases, nucleases, lipases, and hydrolyzing enzymes for polysaccharides to the lumen of phagosomes, are the most pivotal organelles that support phagosomal degradation [3]. The fusion of lysosomes to phagosomes also helps acidify the phagosomal lumen, creating a low pH condition in which the digestive enzymes are active [3]. Besides lysosomes and endosomes, whether other kinds of intracellular organelles fuse to phagosomes and contribute to the degradation of the apoptotic cells inside remains elusive.

Mammalian microtubule-associated protein 1 light chain 3 (MAP1-LC3, or LC3) protein is a member of the ATG8 protein family [4]. LC3 molecules that are conjugated to the lipid phosphatidylethanolamine (PE) are most often observed on the surfaces of autophagosomes, double-membrane organelles that are a key structure of macroautophagy [4]. In fact, LC3 is a well-established marker for autophagosomes [4]. In mammalian cells, lipidated LC3 molecules were also reported to label a novel kind of vesicles referred to as LC3-associated phagocytosis (LAP) vesicles, which are single-membrane vesicles [5]. LAP vesicles were reported to be the third kind of intracellular vesicles that fuse to phagosomes and facilitate the degradation of apoptotic cells in mice [6-8].

Autophagy is an evolutionarily conserved cellular event that plays an essential role in maintaining cellular homeostasis by enveloping harmful protein aggregates and damaged cellular organelles in double-membrane autophagosomes and subsequently degrading them via fusion with lysosomes [9]. Autophagy also supports cell survival during nutrient starvation by capturing intracellular organelles into autophagosomes and converting them to nutrients and energy sources [9]. Autophagosome formation requires the organized action of a set of proteins known as **a**u**t**opha**g**ic related (ATG) proteins. It is a process of three sequential steps: initiation, nucleation, and expansion, until an autophagosome fully forms and closes [10]. After formation, autophagosomes undergo a maturation process through fusion with lysosomes, which provide digestive enzymes to degrade

63 autophagosomal contents [10]. In the nematode *C. elegans*, several autophagy genes have been reported
64 to facilitate the clearance of apoptotic cells [11-13]. However, it is unknown whether autophagosome,
65 as a particular type of cellular organelle, is involved in the clearance of apoptotic cells or whether these
66 *atg* genes have additional functions, such as forming LAP vesicles.

67 Although both are labeled with LC3, mammalian LAP vesicles and autophagosomes are
68 different in several key aspects. First, LAP vesicles are single-membrane vesicles, unlike
69 autophagosomes, which are double-membrane vesicles [5,10]. In addition, although the formation of
70 LAP vesicles relies on a lot of autophagy genes, *ulk1*, *atg13*, and *atg14*, three genes whose products act
71 in the initiation complexes for autophagosomes, are dispensable for the generation of LAP vesicles
72 [5,7,14]. During the initiation of autophagosomes formation, which starts with the appearance of a
73 membrane structure known as a phagophore, ULK1, a serine-threonine kinase, forms a protein complex
74 with ATG13 and two other proteins and phosphorylates the class-III phosphoinositide 3-kinase (PI3K)
75 VPS34 as well as the rest of the VPS34 complex (ATG6, ATG14, and VPS15), triggering the
76 production of PtdIns(3)P on the phagosphore [10]. These distinct features of autophagosomes and LAP
77 vesicles are critical for distinguishing whether an LC3-labeled vesicle is an autophagosome or a LAP
78 vesicle.

79 During *C. elegans* embryonic development, 131 somatic cells undergo apoptosis and are swiftly
80 engulfed and degraded by neighboring cells [15,16]. Apoptotic cells display a "button-like" structure
81 under the Differential Contrast Interference (DIC) microscopy and are referred to as cell corpses [15,16].
82 Mutants defective in the clearance of cell corpses exhibit an increased number of persistent cell corpses,
83 a phenotype known as **ce**ll **d**eath abnormal (Ced) [17]. Previous genetic studies revealed two parallel,
84 partially redundant pathways that primarily drive the clearance of *C. elegans* cell corpses. These include
85 a signaling pathway led by CED-1, a phagocytic receptor for apoptotic cells, CED-6, an adaptor protein
86 for CED-1, and DYN-1, a large GTPase playing many roles in membrane trafficking, and the other
87 pathway led by the small Rac1 GTPase CED-10, and CED-5 and CED-12, the bipartite nucleotide
88 exchange factor for CED-10 [18]. Unlike the CED-10 pathway, which primarily regulates cell corpse
89 engulfment, the CED-1 pathway has two separate functions, regulating both the engulfment and
90 degradation of cell corpses [19]. CED-1 on neighboring engulfing cells recognizes the "eat me" signal
91 on the surfaces of cell corpses and is enriched to the region of the plasma membrane facing a cell corpse
92 [20]. This enrichment initiates the extension of pseudopods along the cell corpse and the subsequent
93 closure of the phagocytic cup to form a nascent phagosome [21,22]. Moreover, CED-1 also plays a
94 distinct role in initiating the degradation of phagosomal contents [19]. CED-1 remains transiently

95 enriched on the surface of nascent phagosomes, where it facilitates the CED-6 and DYN-1-mediated
96 sequential recruitment of the Class II phosphatidylinositol 3-bisphosphate (PtdIns(3)P) kinase PIKI-1,
97 the Class III PtdIns(3)P kinase VPS-34, and the small GTPases RAB-5 and RAB-7 to phagosomal
98 surfaces [19,23]. The robustly produced PtdIns(3)P and the RAB-5 and RAB-7 GTPases further recruit
99 effectors for PtdIns(3)P and the RAB proteins, respectively, which drive the recruitment and fusion of
100 early endosomes and lysosomes to a phagosome, leading to the degradation of the cell corpse inside [23-
101 25]. RAB-7, in particular, is responsible for the fusion of lysosomes to phagosomes [19].
102 Autophagy and phagocytosis are two distinct lysosomal-mediated cellular degradation pathways
103 designated to eliminate intracellular and extracellular components, respectively. Previously, whether
104 canonical autophagosomes were involved in the degradation of phagosomal contents was unknown. We
105 report here that, in *C. elegans* embryos, during the maturation of phagosomes that contain apoptotic
106 cells, LC3-labeled, double-membrane canonical autophagosomes are recruited to phagosomal surfaces
107 and subsequently fuse to these phagosomes. We have further discovered that this event facilitates the
108 degradation of apoptotic cells inside the phagosomal lumen and is driven by the signaling pathway led
109 by CED-1. This autophagosome-phagosome fusion represents a novel mechanism that contributes to the
110 degradation of phagosomal contents.
111

112 ## Results

113 **Vesicles labeled with GFP-tagged LC3 are recruited to the surfaces of phagosomes**

114 The ATG8 protein family is composed of two subfamilies, the LC3 subfamily, and the
115 GABARAP subfamily, which are very close to each other in sequence; the ATG8 family is also referred
116 to as the LC3/GABARAP family [4]. *C. elegans* has two LC3/GABARAP family members, LGG-1 and
117 LGG-2, which belong to the LC3 and GABARAP subfamilies, respectively (**Fig 1A**) [26]. Both LGG-1
118 and LGG-2 are attached to autophagosomes, except that they each label autophagosomes of different
119 maturity [26].
120 To determine whether autophagosomes interact with phagosomes that contain apoptotic cells in
121 *C. elegans* embryos, we constructed the GFP-tagged LGG-1 and LGG-2 reporters that were expressed
122 under the control of the *ced-1* promoter (P_{ced-1}), a well-documented engulfing cell-specific promoter
123 [20,27]. In embryos, we observed numerous GFP::LGG-1$^+$ and GFP::LGG-2$^+$ puncta (**Fig 1**, **D,G**).
124 Using our previously established time-lapse recording protocol [27], we observed the enrichment of
125 GFP::LGG-1$^+$ and GFP-LGG-2$^+$ puncta to the surfaces of the phagosomes, including the phagosomes

126 containing apoptotic cells C1, C2, and C3 (**Fig 1 B, D, G**). These GFP-labeled puncta were not
127 observed inside the phagosomal lumen (**Fig 1 D**, **G**, top panels).
128 *C. elegans* LGG-1 and LGG-2 were both reported to specifically attach to autophagosomes
129 through their lipid tails [26,28]. To verify that the observed GFP puncta are LGG-labeled lipid vesicles
130 and not artifacts of protein aggregation, we tested two mutant constructs, GFP::LGG-1(G116A) and
131 GFP::LGG-2(G130A), which bear mutations in the lipidation sites of the LGG proteins and are deficient
132 for membrane targeting [26]. We found that both GFP::LGG-1(G116A) and GFP::LGG-2(G130A)
133 display a diffuse cytosolic localization pattern **(Fig 1 D**, **G**, bottom panels**)**, in stark contrast to the
134 punctate pattern presented by GFP::LGG-1 and GFP::LGG-2. This result indicates that GFP::LGG-1
135 and GFP::LGG-2 are membrane attached and thus label lipid vesicles.
136
137 **The LGG-tagged puncta that fuse to phagosomes are double-membrane vesicles**
138 The fluorophore within GFP is sensitive to acidic pH (pKa=6.0) [29], thus its signal diminishes
139 when GFP is inside the acidic lumen of lysosomes and phagosomes. To further monitor the fate of the
140 LGG^+ puncta after they are recruited to the surfaces of phagosomes, we replaced GFP with mCherry
141 (pKa<4.5) or mNeonGreen (mNG) (pKa=5.1), both of which are more resistant than GFP to the acidic
142 pH environment [30,31], allowing fluorescence signal inside the phagosomal lumen to be detected. Co-
143 expressed with the mCherry::LGG or mNG::LGG reporter are the CED-1::GFP or PH(hPLCγ)::mRFP
144 reporters, which were used in the time-lapse experiments as markers for the extending pseudopods,
145 allowing us to determine the moment when the pseudopods sealed up and a nascent phagosome was
146 born (**Fig 1 E**, **F**, **H**, **I,** top panels). In time-lapse image series of the clearance of C1, C2, and C3, we
147 found that like the GFP::LGG reporters, the mCherry::LGG and mNG::LGG reporters were enriched on
148 the surfaces of phagosomes; moreover, unlike the GFP::LGG reporters, the mCherry and mNG tagged
149 reporters subsequently entered phagosomal lumen (**Fig 1 E**, **F**, **H**, **I**). The fluorescence signal intensity
150 increases over time with the continuous recruitment of the LGG^+ puncta on phagosomal surfaces (**Fig 1**
151 **E**, **F**, **H**, **I, Movie S1, S2,** and **S3**). We measured the intensity of the mCherry::LGG-1 and
152 mCherry::LGG-2 signal in the center of the C3 phagosomes over time from the start of the phagosome
153 (**Materials and Methods**) (**Fig 1C**) and observed over 10-fold increases of the signal intensity within
154 60 min (**Fig 1J**). The appearance of the membrane-attached mCherry::LGG and mNG::LGG signal in
155 the phagosomal lumen indicates that the LGG^+ vesicles fuse with the phagosomal membrane (**Fig 1K**).
156 They further suggest that these vesicles are composed of double membranes labeled with the LGG
157 reporter molecules on both the outer and inner membranes (**Fig 1K**). If these LGG^+ vesicles were

158 single-membrane, no membrane-attached LGG reporter would end up inside the phagosomal lumen
159 because, as a result of fusion, the reporter molecules will be retained on the phagosomal membrane (**Fig**
160 **1K**). Indeed, when CTNS-1, a lysosomal transmembrane protein, is tagged with mRFP, which is acid-
161 resistant (pKa=4.5 [30]), on its C-terminus, the lysosome-phagosome fusion event resulted in the
162 incorporation of the mRFP signal to the phagosomal membrane; as a result, the CTNS-1::mRFP signal is
163 only observed on the phagosomal surface, not in the phagosomal lumen (**Fig S1**) [19].

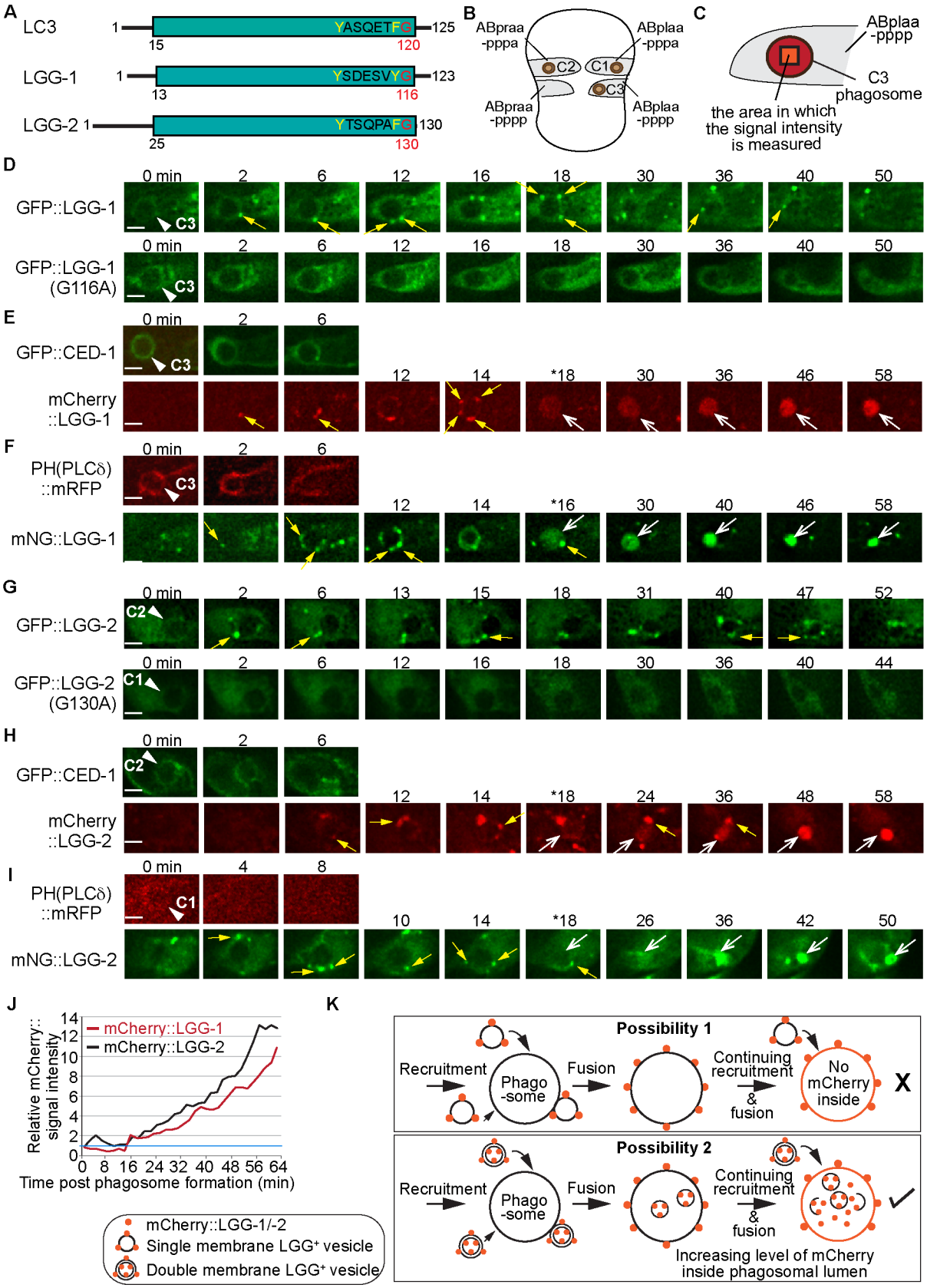

Figure 1. The vesicles labeled with LGG-1 or LGG-2 are recruited to the surface of phagosomes and subsequently fuse to phagosomes.

167 (A) Domain structures of mammalian LC3 and *C. elegans* LGG-1 and LGG-2. The green box indicates
168 the conserved ubiquitin-like domain. Residues in white are conserved among the three proteins. The
169 glycine residue in red is the site where the lipid tail is attached to.
170 (B) A diagram illustrating the three phagosomes that contain cell corpses C1, C2, and C3, with which
171 we monitor the dynamic recruitment and fusion of autophagosomes, at ~330 min post-the 1st embryonic
172 division. Both the positions of C1, C2, and C3 (brown dots) and the identities of their engulfing cells are
173 shown.
174 (C) A diagram illustrating that the relative mNG signal in the center of a phagosome is measured over
175 time to create sub-figure (J). At time point T (time after engulfment), the Relative signal intensity $_T$ =
176 (Unit Intensity(phagosome center)$_T$ – Unit Intensity (background)$_T$) / (Unit Intensity(phagosome
177 center)$_{T0}$ – Unit Intensity(background)$_{T0}$).
178 (D-I) Time-lapse images of indicated reporters starting when a nascent phagosome (white arrowheads)
179 just formed (time point "0 min"). All reporters were expressed under the control of P_{ced-1}. Scale bars are
180 2 μm. Solid white arrowheads label nascent phagosomes. Yellow arrows mark a few LGG-labeled
181 puncta on the surface of phagosomes. Open white arrows in (E, F, H, I) label the phagosomal lumen in
182 which the LGG signal is observed. "*" is the time point when the LGG signal is first seen inside the
183 phagosomal lumen. CED-1::GFP (E, H) and PH(PLCγ)::mRFP (F, I) are co-expressed markers that
184 label the surfaces of nascent phagosomes.
185 (D) GFP::LGG-1-labeled puncta are observed on the surface of a C3 phagosome, but the GFP signal is
186 not seen inside the phagosomal lumen. No GFP::LGG-1(G116A)-labeled puncta are seen on the
187 surface of phagosomes.
188 (E-F) The mCherry::LGG-1 (E) and mNG::LGG-1 (F) puncta are observed on the surface of a C3
189 phagosome and subsequently accumulate inside the phagosome lumen.
190 (G) GFP::LGG-2-labeled puncta are observed to attach on the surface of a C2 phagosome, but the
191 GFP signal does not enter the phagosomal lumen, whereas no GFP::LGG-1(G130A)-labeled puncta
192 are seen on the surface of phagosomes.
193 (H-I) The mCherry::LGG-2 (H) and mNG::LGG-2 (I) puncta are observed on the surface of a C2 (H) or
194 C1 (I) phagosome, respectively, and subsequently accumulate inside the phagosome lumen.
195 (J) The relative mCherry::LGG-1 or -2 signal intensity in the center of a phagosome (Y-axis) over time
196 (in 2-min interval) (X-axis). "0 min" indicates the moment when a nascent phagosome just formed. One
197 blue horizontal line indicates value "1", where no signal enrichment above background level is
198 observed.
199 (K) A diagram illustrating that those double membrane-vesicles labeled with mCherry::LGG on their
200 outer and inner membranes are recruited to phagosomal surfaces and fused to the phagosomal
201 membrane. After the fusion between the outer membrane of these vesicles and phagosomal

202 membrane, the mCherry::LGG-tagged inner membrane enters the phagosomal lumen. The continuing
203 incorporation of these double-membrane vesicles to phagosomes increases the mCherry signal level in
204 the phagosomal lumen, observed over time. If the LGG-1 or LGG-2-labeled vesicles are of a single
205 membrane, no fluorescence signal is expected to enter the phagosomal lumen.
206
207 **The LGG$^+$ vesicles that are incorporated into phagosomes are canonical autophagosomes**
208 The observation that the LGG$^+$ vesicles incorporated into phagosomes are likely double-
209 membrane vesicles reminded us of canonical autophagosomes rather than LAP vesicles. To further
210 determine whether these vesicles represent canonical autophagosomes, we examined whether loss-of-
211 function mutations of *atg-7*, *atg-13*, and *epg-8*, which are defective for the biogenesis of
212 autophagosomes [32,33], impaired the production of these vesicles. *C. elegans atg-13* and *epg-8* encode
213 homologs of mammalian ATG13 and ATG14, respectively, which are essential for the biogenesis of
214 autophagosomes but dispensable for that of LAP vesicles (**Introduction**) [34]. *atg-7* encodes a
215 homolog of mammalian ATG7, a protein essential for conjugating a phospholipid tail onto the LC3
216 family proteins and required for the biogenesis of both autophagosomes and LAP vesicles [10,34]. We
217 first scored whether the mCherry::LGG-1/-2 reporters were observed in the center of 15 phagosomes
218 during the phagosome maturation process (**Figs 1C** and **2**), which is indicative of the fusion of double-
219 membrane mCherry::LGG $^+$ vesicles to phagosomes. In wild-type embryos, the steady entry of mCherry
220 into phagosomes over time (**Fig 1 E**, **H**) results in the increase of the average mCherry::LGG-1 and -
221 LGG-2 intensities to 9.2- and 8.4-fold of that at 0 min time point, respectively, at 60 min after the
222 formation of a phagosome (**Fig 2 H**, **J**). However, in *atg-7(bp411)* [35] mutant embryos, hardly any
223 mCherry signal was observed inside phagosomes **(Fig 2 A, D, G-J)**. At 60 min after the phagosome
224 formation, the average mCherry signal intensities were merely 1.2 and 1.4-fold at 0 min time point **(Fig**
225 **2 H, J).** These observations indicate a lack of LGG$^+$ vesicles that fuse to phagosomes. In *atg-*
226 *13(bp414)* and *epg-8(bp251)* mutant embryos, similar observations were made except that the defects
227 were slightly weaker (**Fig 2 B, C, E, F, G-J**).
228 We next examined whether the mCherry::LGG-1/-2$^+$ vesicles are produced in cells of the *atg-7*,
229 *atg-9*, *atg-13*, and *epg-8* mutant embryos. In wild-type embryos at mid-embryonic developmental stages
230 (~330, ~350, ~400 min post-1st embryonic cell division), numerous mCherry$^+$ puncta were observed
231 (**Figs S2A, S3A**). In the *atg-7* mutant embryos, rarely any such puncta existed (**Figs S2B, S3B**),
232 consistent with a previous report [32]. *atg-9* encodes ATG-9, the only transmembrane protein in the
233 core autophagy machinery [32,34]. ATG9 plays an essential role in the expansion of phagophore and
234 the biogenesis of autophagosomes [10]. In *atg-9(bp564)* mutant embryos that expressed mNG::LGG-1

235 or ::LGG-2, much fewer mNG$^+$ puncta that might represent autophagosomes were observed, and the
236 mNG reporters label large aggregates (**Fig S4**), consistent with a previous report [36]. In *atg-13* and
237 *epg-8* mutant embryos, the numbers of mCherry-LGG$^+$ puncta were also significantly reduced (**Figs S2**
238 **C-D, S3 C-D**), suggesting that the *atg-13(bp414)* and *epn-8(bp251)* mutations severely impaired the
239 biogenesis of autophagosomes, a phenotype that is consistent with previous reports [32,33]. The drastic
240 reduction in the number of LGG-1/-2-labeled puncta in *atg-7*, *atg-9, atg-13,* and *epg-8* loss-of-function
241 mutants strongly indicate that these puncta belong to canonical autophagosomes.

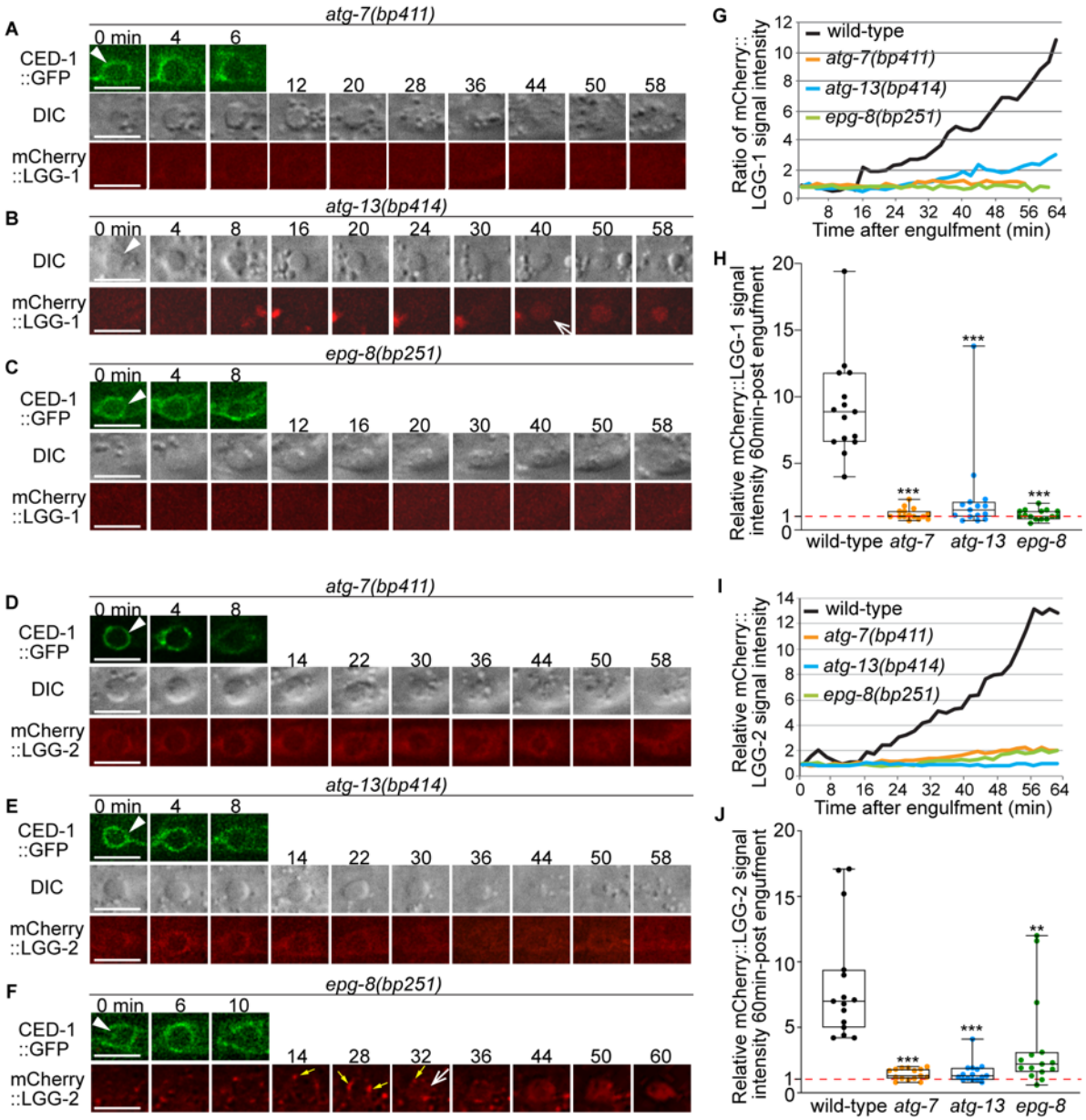

242
243 **Figure 2. In autophagosome-formation mutants, the enrichment of the LGG$^+$ vesicles on the**
244 **phagosomal surface and the entry of the LGG signal into the phagosomal lumen are both**
245 **severely defective.**

246 (A-F) Time-lapse image series monitoring the enrichment of the puncta labeled with mCherry-tagged
247 LGG-1 (A-C) or LGG-2 (D-F) on phagosomes (white arrowheads) and the subsequent entry of mCherry
248 signal into the phagosomal lumen in *atg-7*, *atg-13*, and *epg-8* mutant embryos. DIC images mark the
249 position of the cell corpse. "0 min" is when a phagosome is just sealed (determined by CED-1::GFP). "*"
250 denotes the time point that the mCherry signal starts to appear inside the phagosomal lumen. Scale
251 bars are 2μm. Yellow arrows in (F) mark mCherry::LGG-2 puncta on the surface of a phagosome
252 (open white arrow).
253 (G and I) The relative mCherry::LGG-1 or -2 signal intensity in the center of a phagosome (Y-axis) over
254 time (in 2-min interval) (X-axis). "0 min" indicates the moment when a phagosome is just sealed. (G)
255 The data for the wild-type, *atg-7(bp411)*, *atg-13(bp414)*, and *epg-8(bp251)* mutant embryos are from
256 Figures 1E and 2(A-C), respectively. (I) The data for the wild-type, *atg-7(bp411)*, *atg-13(bp414)*, and
257 *epg-8(bp251)* mutant embryos are from Figures 1I and 2(D-F), respectively.
258 (H and J) Box-and-Whiskers plots of the relative mCherry signal intensity measured in the center of
259 phagosomes 60 min-post the formation of nascent C3 phagosomes from 15 each of wild-type, *atg-*
260 *7(bp411)*, *atg-13(bp414)*, and *epg-8(bp251)* mutant embryos. Red dashed lines indicate the position of
261 value 1, which represents no signal enrichment relative to the background signal.
262 ***, $p<0.001$, **, $<0.001p<0.01$, Student *t*-test of each mutant comparing to the wild-type value.
263
264 To further confirm that autophagosomes fuse to phagosomes, we examined the subcellular
265 localization of a mCherry::ATG-9 reporter expressed in engulfing cells. Besides the LGG proteins,
266 ATG-9 is also an established autophagosomes marker as it is the only transmembrane protein in
267 autophagosomes [37]. In embryonic hypodermal cells that co-expressed mCherry::ATG-9 and either
268 mNG::LGG-1 or::LGG-2, puncta labeled with mCherry are recruited to the surfaces of phagosomes (**Fig**
269 **3**). Furthermore, the mCherry signal gradually accumulates in the phagosomal lumen like the LGG
270 reporters (**Fig 3**). During the phagosome maturation process, the co-localization between
271 mCherry::ATG-9 and each of the two LGG reporters on the puncta on phagosomal surfaces and inside
272 phagosomal lumen was nearly perfect (**Fig 3**). Together, the above observations verified that
273 autophagosomes on which membranes ATG-9 and LGG proteins are present are recruited to
274 phagosomal surfaces and subsequently fuse to phagosomes containing apoptotic cells.

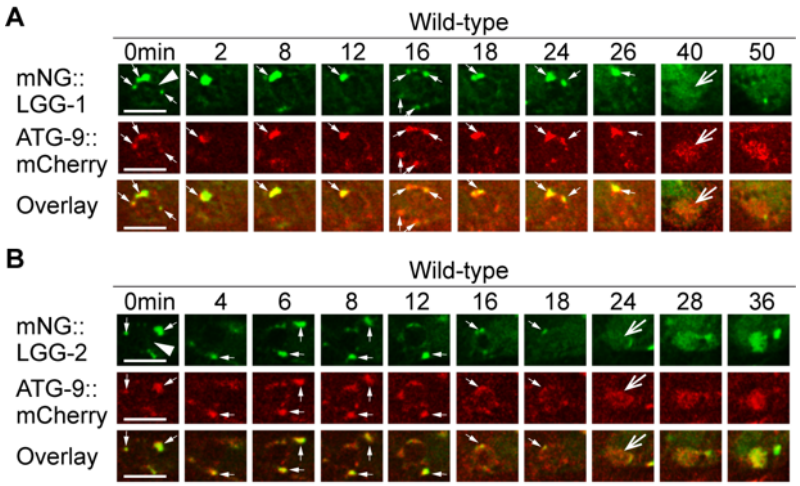

Figure 3. LGG-1 and LGG-2$^+$ puncta colocalize with ATG-9, a component of autophagosomes. The mNG- and mCherry-tagged reporters are expressed in wild-type embryos under the control of P_{ced-1}. White arrowheads make nascent phagosomes. Small white arrows mark the regions where LGG$^+$ and ATG-9$^+$ puncta colocalize. Open white arrows indicate the moment when the fluorescent signal is first detected inside the phagosomal lumen. Scale bars are 5 μm.

(A) Time-lapse microscopy showing the localization of mNG::LGG-1 and mCherry::ATG-9. Images are from ABplaapppp, which engulfs C3.

(B) Time-lapse microscopy showing the localization of mNG::LGG-2 and mCherry::ATG-9. Images are from ABplaapppa, which engulfs C1.

Autophagosomes facilitate the degradation of apoptotic cells inside phagosomes

To examine whether the incorporation of autophagosomes into phagosomes affects the clearance of the engulfed apoptotic cells, we first quantified whether, in mutants of genes essential for the biogenesis of autophagosomes, apoptotic cells were un-degraded and persistent in embryos. In addition to the *atg-7*, *atg-9*, *atg-13*, and *epg-8* mutants characterized above, we also characterized loss-of-function mutants of *lgg-1* and *lgg-2*, and of *atg-3*, whose gene product is essential for the conjugation of a PE tail to the LC3 family proteins [32,38], of *atg-2* and *atg-18*, whose gene products function together with ATG-9 in the expansion of phagophore [37], and of *unc-51*, which encodes a *C. elegans* homolog of ULK1, an autophagic protein kinase [37]. In 2-fold stage wild-type embryos, which are ~460 min post the first embryonic cell division, an average of 11.3 cell corpses were scored (**Fig 4A**). The mutant 2-fold embryos examined bore 46.9% - 91.2% more cell corpses (**Fig 4)**, indicating that the clearance of cell corpses is defective. Together, the findings reported in **Figs 2**, **3**, and **4** indicate that autophagosomes made a substantial contribution to the clearance of cell corpses.

299 To determine whether the lack of autophagosomes impairs the engulfment or degradation of cell
300 corpses, we monitored the formation and degradation of phagosomes containing apoptotic cells C1, C2,
301 and C3 (**Fig 1B**) in wild-type, *atg-7*, and *lgg* mutant embryos in real-time using established protocol
302 **(Materials and Methods)** [24,27]. The CED-1::GFP expressed in engulfing cells labels the extending
303 pseudopods and enables us to monitor the process of phagosome formation, starting from the budding
304 and ending at the sealing of the pseudopods [20,21]. 2xFYVE::mRFP (also expressed under P_{ced-1}), a
305 reporter for phagosomal surface PtdIns(3)P, enables us to monitor the shrinking of a phagosome, an
306 indication of phagosome degradation [19,23,24]. In *atg-7*, *lgg-1,* and *lgg-2* mutant strains that co-
307 expressed CED-1::GFP and 2xFYVE::mRFP, we found that engulfment was completed in 4-8 min, just
308 like in wild-type embryos (**Fig 5 A-E**), indicating that defects in autophagosomes biogenesis do not
309 affect the engulfment of cell corpses. However, the lifespans of phagosomes (**Materials & Methods**)
310 were much longer in *atg-7*, *lgg-1*, and *lgg-2* mutants than in wild-type embryos (**Fig 5 A-D, F**). All
311 wild-type phagosomes have a lifespan between 40-60 min (**Fig 5F**). In *atg-7*, *lgg-1,* and *lgg-2* mutants,
312 the lifespan varied in a much more extensive range. Remarkably, 43.8%, 53.3%, and 82.4% of
313 phagosomes in *atg-7*, *lgg-2,* and *lgg-1* mutant embryos, respectively, have lifespans longer than 60 min
314 (**Fig 5F**). The longest persisting phagosome, which was observed in an *lgg-1* mutant embryo, lasted
315 longer than 136 min (**Fig 5D**). These observations indicate that autophagosomes made a specific
316 contribution to the efficient degradation of phagosomal contents.

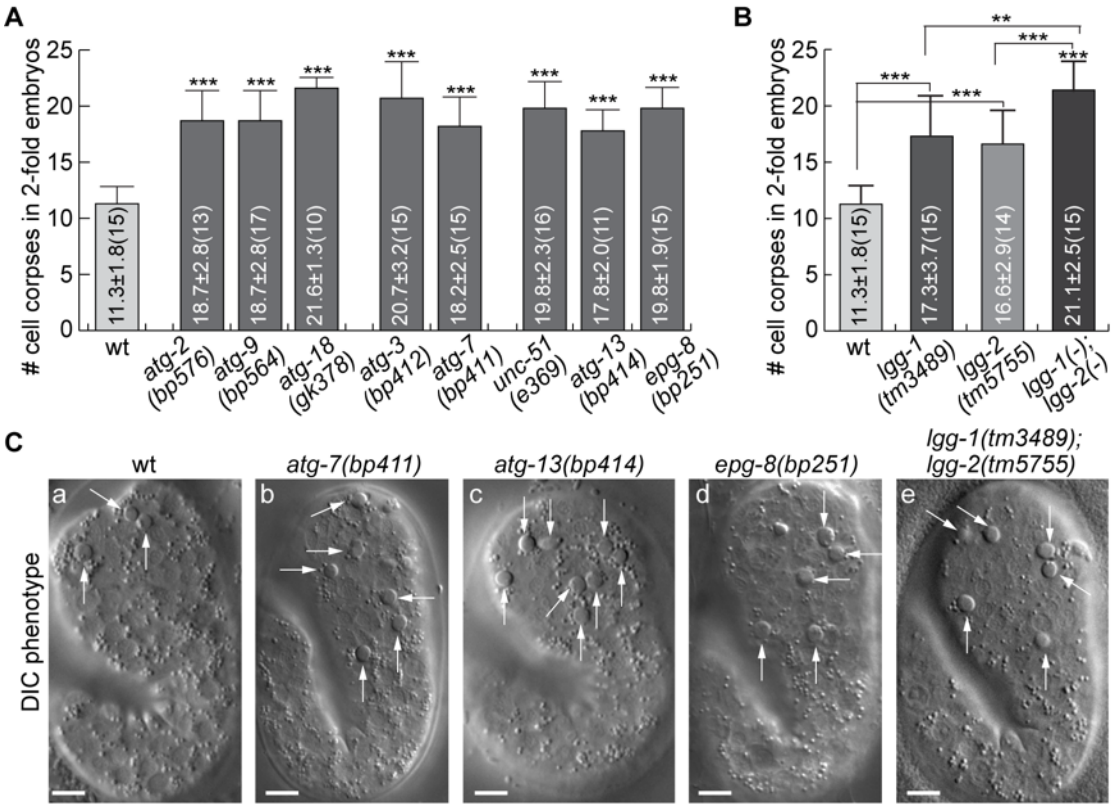

Figure 4. Mutations in autophagy genes impair the clearance of apoptotic cells.

(A-B) Bar graph displaying the average numbers of somatic cell corpses in 2-fold stage wild-type and various mutant embryos. Bars and error bars represent mean and standard deviation (sd), respectively, the actual values of which are displayed inside the bars. Numbers in parentheses indicate the number of embryos scored. ***, $p<0.001$, Student *t*-test of each mutant comparing to the wild-type value.

(C) DIC images of cell corpses in 2-fold stage embryos of various genotypes. White arrows indicate button-like structures characteristic of cell corpses. Scale bars are 5 μm.

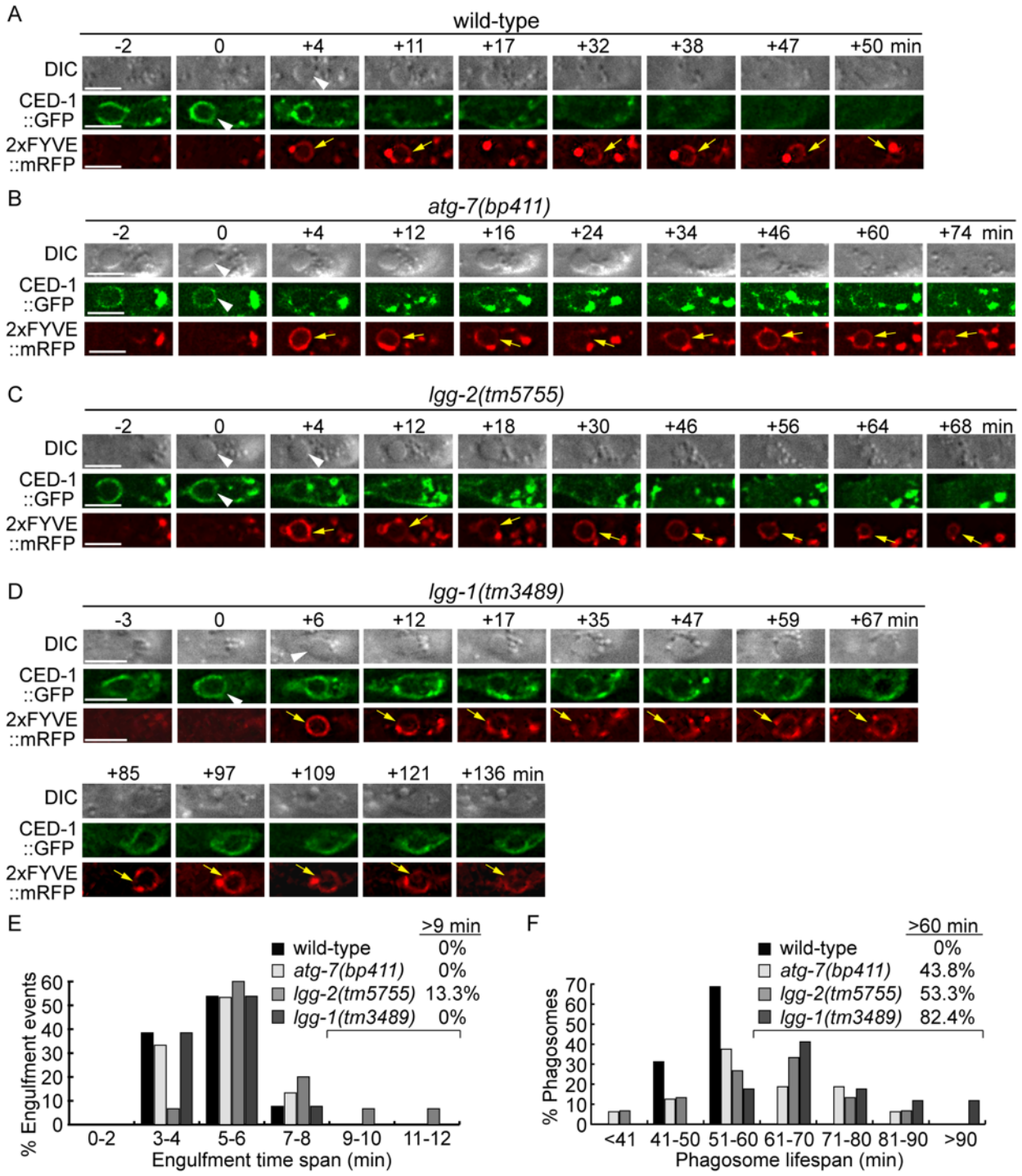

Figure 5. Mutations in *atg-7*, *lgg-1,* and *lgg-2* delay the degradation of cell corpses. (A-D) Time-lapse recording conducted in wild-type and different mutant embryos monitoring the dynamics of the pseudopod marker CED-1::GFP and the phagosome marker 2xFYVE::mRFP (both expressed in engulfing cells) during the engulfment and degradation processes of cell corpse C3 by ABplaapppp. “0 min” is the first time point when a nascent phagosome (white arrowheads) is formed, as indicated by the closure of a green GFP::CED-1 ring. 2xFYVE::mRFP labels the surface of a phagosome (yellow arrows) until it is degraded. Scale bars are 2 μm.

335 (E) Histogram depicting the distribution of the time it takes to engulf 15 C3 cell corpses in each of the
336 four genotypes. The engulfment time is defined as the period between the first time point when
337 pseudopods (labeled with CED-1::GFP) are spotted and the time point when a full circle forms around
338 C3.
339 (F) Histogram depicting the distribution of the duration of 15 C3 phagosomes in each of the four
340 genotypes. Phagosome lifespan is measured as the time interval between the "0 min" time point and
341 the time point when the phagosome shrinks to one-half of its original diameter.
342

343 **LGG-1 and LGG-2 act in engulfing cells, and together they define three subpopulations of**
344 **autophagosomes that are incorporated into phagosomes**

345 LGG-1 and LGG-2 have distinct structural features and were observed to attach to different sub-
346 populations of autophagosomes, which represent autophagosomes at different maturation stages [26,28].
347 The sub-populations of autophagosomes labeled by LGG-1- or LGG-2- are incorporated into
348 phagosomes (**Fig 1**). *lgg-1* and *lgg-2* single mutants are both inefficient in clearing cell corpses (**Fig**
349 **4B**). Furthermore, in *lgg-1; lgg-2* double mutant embryos at 2-fold, the Ced phenotype is further
350 enhanced significantly (**Fig 4B**) -- the number of cell corpses is 22.0% and 27.1% larger than in the *lgg-*
351 *1* and *lgg-2* single mutants, respectively. This enhanced phenotype indicates an additive effect and
352 suggests that the autophagosomes labeled with LGG-1 or LGG-2 play parallel and partially redundant
353 roles in promoting phagosome degradation. In embryos co-expressing GFP::LGG-1 and
354 mCherry::LGG-2, we observed that on the surfaces of phagosomes, those puncta were either labeled
355 with GFP mCherry alone or with both GFP and mCherry (**Fig 6A**). In hypodermal cells, puncta that
356 were either labeled with GFP mCherry alone or with both GFP and mCherry but were not attached to
357 phagosomes were also observed (**Fig 6B**). These observations indicate that in addition to the LGG-1^+-
358 only and LGG-2^+-only subpopulations, a third LGG-1^+ LGG-2^+ double-positive subpopulation of
359 autophagosomes exists. This subpopulation likely corresponds to an intermediate stage during the
360 maturation path of autophagosomes.

361 To determine whether LGG-1 and LGG-2 act in engulfing cells to facilitate phagosome
362 degradation, we examined whether the specific expression of each gene in engulfing cells, under the
363 control of P_{ced-1}, would rescue the Ced phenotype of the corresponding mutant embryos. We tested both
364 the *gfp*- and *mCherry*-tagged *lgg* cDNAs for the rescuing activity by counting the number of cell corpses
365 in 1.5-fold stage transgenic embryos. In the *lgg-1* and *lgg-2* null mutants, both the *gfp*- and *mCherry*-
366 tagged corresponding *lgg* cDNA efficiently rescued the Ced phenotype (**Fig S5**). The *gfp::lgg-1* and
367 *mCherry::lgg-1* transgenes lowered the number of cell corpses from on-average 152% of wild-type level

368 observed in the *lgg-1(tm3489)* mutants to 118% and 123% of the wild-type level, respectively.
369 Similarly, the *gfp::lgg-2* and *mCherry::lgg-2* transgenes lowered the number of cell corpses from on-
370 average 143% of wild-type level observed in the *lgg-2(tm5755)* mutants to 109% and 112% of the wild-
371 type level, respectively (**Fig S5**). These results indicate that *lgg-1* and *lgg-2* primarily act in engulfing
372 cells to facilitate the clearance of apoptotic cells.

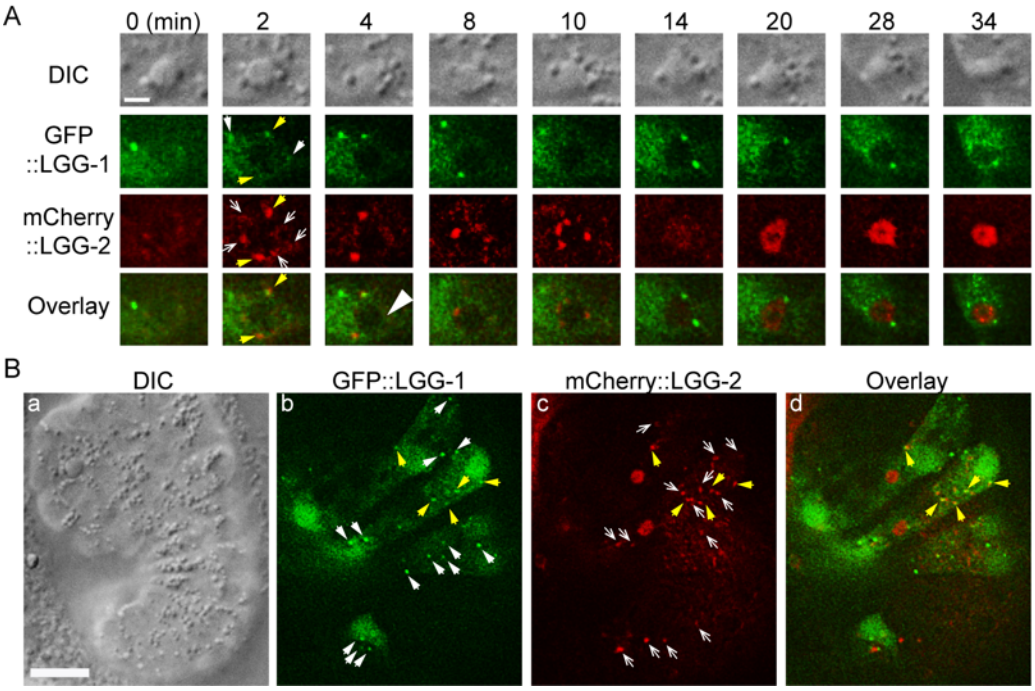

373

374 **Figure 6. The puncta labeled with LGG-1 and/or LGG-2 define three distinct populations of**
375 **vesicles**
376 The time-lapse recording was conducted on wild-type embryos co-expressing P_{ced-1}*gfp::lgg-1* and P_{ced-1}*mCherry::lgg-2*.
378 (A) Time-lapse image series of a C2 phagosome (one big white arrowhead in the "4 min" image). "0
379 min" is the moment when a nascent phagosome just seals. The scale bar is 2 μm. The white arrows,
380 white open arrows, and yellow arrows in the "2 min" image panels mark GFP^+ $mCherry^-$, GFP^-
381 $mCherry^+$, and GFP^+ $mCherry^+$ puncta on the surface of the phagosome, respectively.
382 (B) DIC and fluorescence images of an embryo exhibiting LGG^+ puncta outside phagosomes in multiple
383 cells. The scale in (a) bar is 10 μm. The white arrows, white open arrows, and yellow arrows mark
384 GFP^+ $mCherry^-$, GFP^- $mCherry^+$, and GFP^+ $mCherry^+$ puncta on the surface of the phagosome,
385 respectively.
386

387 **The small GTPase RAB-7 and the HOPS complex are essential for the fusion between**
388 **autophagosomes and phagosomes**

389 The small GTPase RAB-7 is recruited to the phagosomal membrane shortly after the formation
390 of a *C. elegans* phagosome [19]. RAB-7 is also enriched on the surface of lysosomes [19]. Mammalian
391 RAB7 and *C. elegans* RAB-7 mediate the fusion between the maturing phagosome and lysosomes and
392 do that through their effector, the HOPS complex [3,25,39]. In addition, mammalian RAB7 is known to
393 drive lysosome-autophagosome fusion through the HOPS complex and PLEKHM1, an adaptor protein
394 [40,41]. *C. elegans* RAB-7 also plays an essential role in autolysosome formation [26], although
395 whether it is localized to autophagosomes was not reported previously. To examine whether RAB-7 is
396 localized to LGG-1$^+$ and LGG-2$^+$ autophagosomes that fuse to *C. elegans* phagosomes, we generated
397 two transgenic *C. elegans* strains that co-expressed the mCherry::LGG-1/ GFP::RAB-7 or
398 mCherry::LGG-2/ GFP::RAB-7 pairs of reporters (**Materials and Methods**). We observed that
399 GFP::RAB-7 was localized to some but not all of the LGG-1$^+$ or LGG-2$^+$ puncta (**Fig 7 B-D**). The
400 LGG$^+$ RAB-7$^+$ double-positive autophagosomes were observed both freely distributed in the cytoplasm
401 of ventral hypodermal cells (**Fig 7B(a-c)** and **C**) and on phagosomal surfaces (**Fig 7B(d-f)**, **D**). In
402 addition, **Fig 7B(d-f)** depicts that GFP::RAB-7 is both evenly distributed to the surface of a phagosome
403 (d) as previously reported [19], and highly enriched on LGG-1$^+$ autophagosomes that are recruited to
404 the phagosomal surface (**d-f**, white arrows). **Fig 7D** shows a dynamic fusion event of an LGG-2$^+$/RAB-
405 7$^+$ punctum (marked by the bottom arrow in the "0 min" time point) attached to the phagosome
406 membrane and becoming part of the phagosomal surface at the "+6 min" time point. On the other hand,
407 we also observed puncta that were LGG$^+$ but RAB-7$^-$ (Fig 7 B and C, white arrowheads), which were
408 likely autophagosomes not acquired RAB-7 yet, and puncta that were LGG$^-$ but RAB-7$^+$ (Fig 7 B and C,
409 yellow arrows), which represented intracellular organelles such as late endosomes or lysosomes. In
410 conclusion, RAB-7 is localized to the majority but not all autophagosomes; furthermore, all
411 autophagosomes that were observed on phagosomal surfaces were RAB-7$^+$.
412 We next examined whether the recruitment and fusion of LGG-1$^+$- or LGG-2$^+$- autophagosomes
413 to the C1, C2, and C3 phagosomes were normal in *rab-7(ok511)* null mutant embryos [19]. The
414 enrichment of mCherry$^+$ puncta on the surfaces of phagosomes indicates the recruitment event, whereas
415 the accumulation of the mCherry signal inside the phagosomal lumen indicates the fusion event. In *rab-*
416 *7(ok511)* mutants, robust enrichment of both the mCherry::LGG-1$^+$ and ::LGG-2$^+$ puncta to phagosomal
417 surfaces are prominent (**Fig 7 E-F**), indicating that the recruitment of autophagosomes was normal.
418 However, no mCherry signal was observed entering the phagosomal lumen (**Fig 7 E-F, Movies S4, S5**).
419 We quantified the time between the moments a phagosome was just born and that when an obvious
420 mCherry signal was observed inside the phagosomal lumen. In the wild-type embryos, this time is <30

421 min in 100% of the samples analyzed, and the median value is 14 and 18 min for LGG-1$^+$ and LGG-2$^+$
422 autophagosomes, respectively (**Figs 1**(**E** and **H**) and **7(G-H)**). In stark contrast, in *rab-7* mutants, the
423 mCherry signal was not detected in the lumen inside any of the phagosomes for LGG-1 or LGG-2
424 reporters (n=9 for each reporter) over a time span of 0-60 min after phagosome formation (**Fig 7 G-H**).
425 For over half of the samples, the observation period was extended beyond 90 min after phagosome
426 formation, and still, no mCherry signal was observed in the phagosomal lumen within this period.
427 These results strongly indicate that RAB-7 function is absolutely needed for
428 autophagosomes/phagosome fusion but not required for the recruitment of autophagosomes to
429 phagosomal surfaces.
430 In *C. elegans*, a null mutation in *vps-18*, which encodes VPS-18, a subunit of the HOPS
431 complex, impairs phagosome maturation [42]. The lack of autophagosome-phagosome fusion observed
432 in *rab-7* mutants hinted us to subsequently examine the *vps-18* null mutant embryos. We found that,
433 like in *rab-7* mutants, the recruitment of autophagosomes to phagosomes appeared normal in *vps-18*
434 mutants (**Fig 7 E-F**). Also, like in *rab-7* mutants, in *vps-18* mutants, the fusion of LGG-1$^+$ and LGG-2$^+$
435 autophagosomes to phagosomes was severely defective (**Fig 7 E-H**). However, whereas in *rab-7*
436 mutants, the entry of mCherry signal to phagosomal lumen was blocked completely in all samples, in
437 some *vps-18* mutant embryos, the entry of mCherry signal still occurred, *albeit* severely delayed. In
438 contrast, in other samples, the entry was blocked **(Fig 7 E-H)**, indicating a fusion defect that is less
439 severe than that caused by the *rab-7* null mutation and suggesting the existence of the residue HOPS
440 function in *vps-18* mutants. Together, our above observations indicate that RAB-7 and the HOPS
441 complex play a critical and specific role in the fusion between autophagosomes and phagosomes.
442

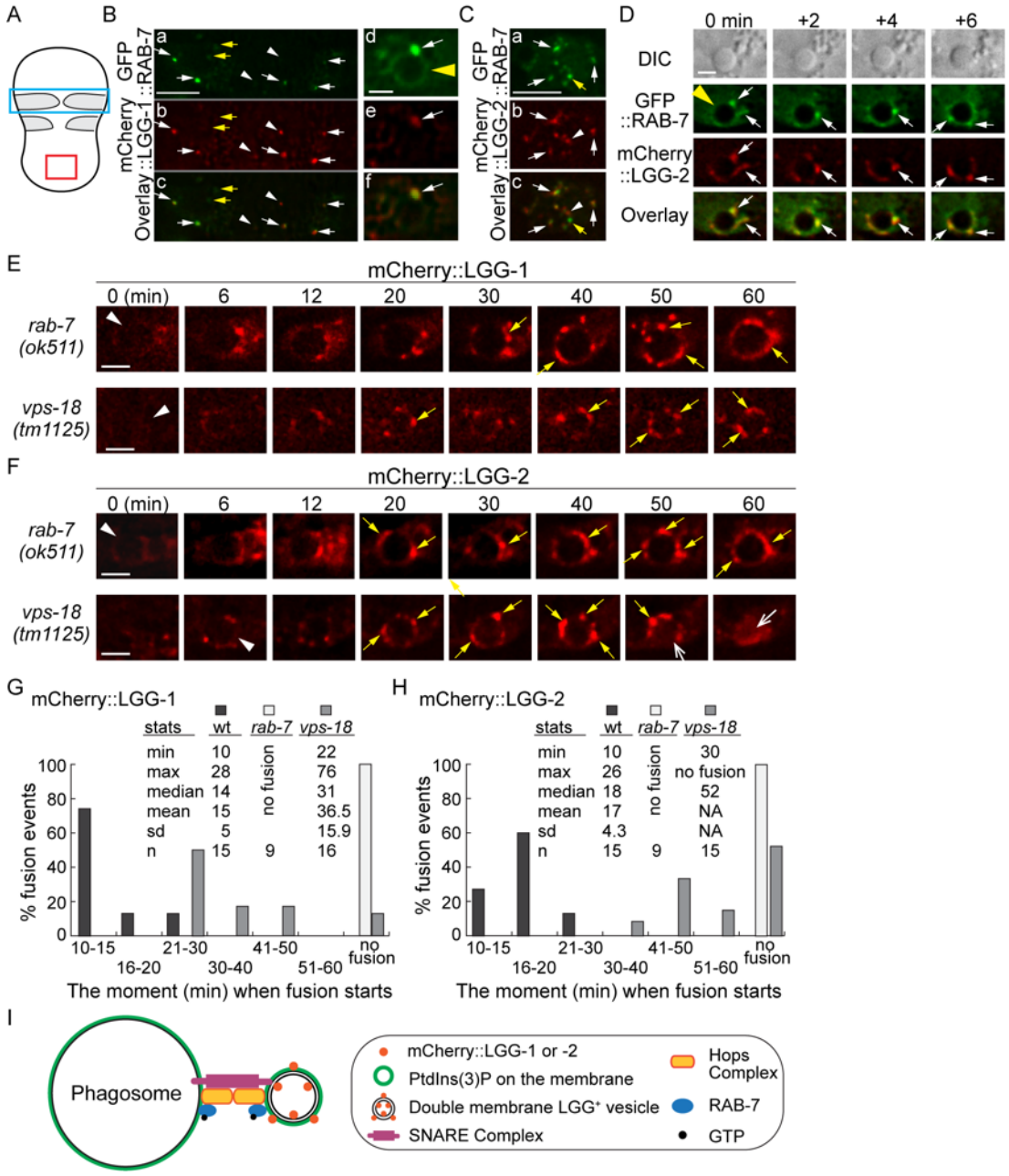

Figure 7. RAB-7 and VPS-18 are essential for the fusion between autophagosomes and phagosomes.

(A) Diagram of the ventral surface of an embryo at ~330 min post 1st embryonic division. (B-D) Images of part of the ventral surface of an embryo co-expressing $P_{ced\text{-}1}$*gfp::rab-7* and $P_{ced\text{-}1}$*mCherry::lgg-1* (B) or $P_{ced\text{-}1}$*mCherry::lgg-2* (C-D). B(a-c) depicts the region framed by the blue box in (A). B(d-f) depicts a C1 phagosome (a yellow arrowhead). C(a-c) depicts the region framed by the red box in (A). (D) A time-lapse image series of a C1 phagosome (a yellow arrowhead) indicates the dynamic recruitment and fusion of GFP and mCherry double-positive puncta to the phagosomal membrane. "0 min" is the moment when the first puncta are observed on the phagosomal surface. White arrows mark several puncta that are both GFP$^+$ and mCherry$^+$. Yellow arrows mark puncta that

454 are GFP$^+$ but mCherry$^-$. White arrowheads mark puncta that are GFP$^-$ but mCherry$^+$. Scale bars for
455 B(a-c) and (C) are 5 μm, and for B(d-f) and (D) are 2 μm.
456 (E-F) Time-lapse images monitoring the recruitment and fusion of puncta labeled with mCherry::LGG-1
457 (E) or::LGG-2 (F) to the C1, C2, and C3 phagosomes in *rab-7(ok511)* and *vps-18(tm1125)* mutant
458 embryos. "0 min" represents the moment when a phagosome just seals (white arrowheads). Yellow
459 arrows mark the mCherry$^+$ puncta on the phagosomal surfaces. One open white arrow marks the
460 mCherry signal inside the phagosomal lumen. Scale bars are 2 μm.
461 (G-H) Histograms depicting the distribution of the time it takes for LGG-1$^+$ or LGG-2$^+$ puncta to fuse to
462 phagosomes, measured from the "0 min" point to the time point when mCherry was detected in the
463 center of a phagosome. C1, C2, and C3 phagosomes were recorded. *n*, the number of phagosomes
464 scored. "No fusion": no mCherry signal entry was observed even after 72-114 min post-nascent
465 phagosome formation. NA: not applicable.
466 (I) A Diagram depicting the mechanism driving autophagosome-phagosome fusion. RAB-7 is enriched
467 on the surfaces of both phagosomes and autophagosomes. RAB-7 and VPS-18, a subunit of the HOPs
468 complex, are proven essential for autophagosome-phagosome fusion. Other factors are proposed to
469 play roles in this event based on the knowledge of intracellular membrane fusion in general.
470

471 **The CED-1 pathway drives the recruitment of autophagosomes to phagosomes**

472 The signaling pathway led by the phagocytic receptor CED-1 plays essential roles in initiating
473 the maturation of phagosomes containing apoptotic cells [19]. The CED-1 pathway is known to drive
474 the incorporation of early endosomes and lysosomes to phagosomes [19,21]. Here we further examined
475 whether the loss-of-function mutations in members of the CED-1 pathway affect the incorporation of
476 autophagosomes to phagosomes. In *ced-1(e1735)* null mutant embryos [20] that express the
477 mNG::LGG-1 or -2 reporters, we observed severe defects in the incorporation of autophagosomes into
478 phagosomes. First of all, only a very dim mNG signal was observed inside the phagosomal lumen 50
479 min post phagosome formation, a time point well past the observed initiation time for
480 autophagosomes/phagosome fusion in the wild-type condition (**Fig 8 A**, **C**, **F**, and **G, Movie S6**).
481 Whereas in wild-type embryos, the median relative LGG-1 and -2 signal intensities are 6.3 and 5.3 at 50
482 min-post phagosome formation, respectively, in *ced-1* mutant embryos, the median values are merely
483 2.1 and 1.6, respectively (**Fig 8 K-L**). Secondly, unlike in *rab-7* mutants, where autophagosomes were
484 observed accumulating on phagosomal surfaces (**Fig 7**), in *ced-1* mutants, very few LGG-1- or LGG-2-
485 labeled puncta were observed on phagosomal surfaces (**Fig 8 A**, **C**).
486 Further quantitative measurement of the samples presented in (**Fig 8 A**, **C**) and 14 additional
487 samples for each of the reporters confirmed that the mNG signal was not enriched on the surfaces of

488 phagosomes, in contrast to wild-type embryos (**Fig 8 H-L**). These results indicate a severe defect in the
489 recruitment of autophagosomes to phagosomes. Unlike in the *atg* mutants that we have examined (**Figs**
490 **S2** and **S3**), in *ced-1* mutant embryos, normal numbers of LGG-1$^+$ or LGG-2$^+$ puncta were observed
491 (**Fig S6**), indicating that the biogenesis of autophagosomes is normal. Thus the recruitment defect
492 observed in *ced-1* mutants is not a consequence of the lack of autophagosomes; rather, it is likely a
493 result of a defect in signaling between phagosomes and autophagosomes.

494 We further examined whether CED-6 and DYN-1, two other members of the CED-1 pathway,
495 were also needed for the incorporation of autophagosomes into phagosomes. In the *ced-6(n2095)* and
496 *dyn-1(n4039)* mutant embryos, the median relative LGG-1 and LGG-2 signal intensities in the center of
497 phagosomes are much lower than that in wild-type samples, respectively, at 50 min-post phagosome
498 formation mutants (**Figs 8(B, D, F, G, K-L)** and **9(A, D E, F, I, J)**), although the defects are not as
499 severe as in *ced-1* mutants (**Fig 8(A, C, F, G, K, L)**). Further observation discovered that the LGG-1 or
500 LGG-2-labeled puncta were rarely observed on the surfaces of phagosomes in these mutants (**Figs 8(B,**
501 **D, I, J)** and **9(A, F)**), demonstrating severe defects in the recruitment of autophagosomes to phagosomal
502 surfaces.

503 In *ced-1*, *ced-6*, and *dyn-1* mutants, the fusion between autophagosomes and phagosomes might
504 also be defective. However, the severe recruitment defects resulted in the lack of LGG-labeled puncta
505 on phagosomal surfaces, making it difficult to evaluate whether there are additional fusion defects and
506 how severe the fusion defects are.

507 We also examined whether the pathway composed of the small GTPase CED-10 and its bipartite
508 Guanine Nucleotide Exchange Factor (GEF) CED-5 and CED-12, which acts parallel to the CED-1
509 pathway in the engulfment of cell corpses, plays any role in promoting the incorporation of
510 autophagosomes into phagosomes. In the *ced-5(n1812)* null mutant and *ced-10(n1993)* loss-of-function
511 mutant embryos, the accumulation of the LGG-1 and LGG-2 signals on the surfaces of the phagosomes
512 and the subsequent accumulation of signals inside phagosomal lumen were normal both in the time
513 course and in the levels of signal enrichment (**Fig 9 B, C-E, G, H-J**), indicating that both the
514 recruitment and fusion of autophagosomes to phagosomes are normal. We thus conclude that, unlike the
515 CED-1/-6/DYN-1 pathway, the CED-5/-10 pathway is not involved in regulating the incorporation of
516 autophagosomes to phagosomes (**Fig 9K**).

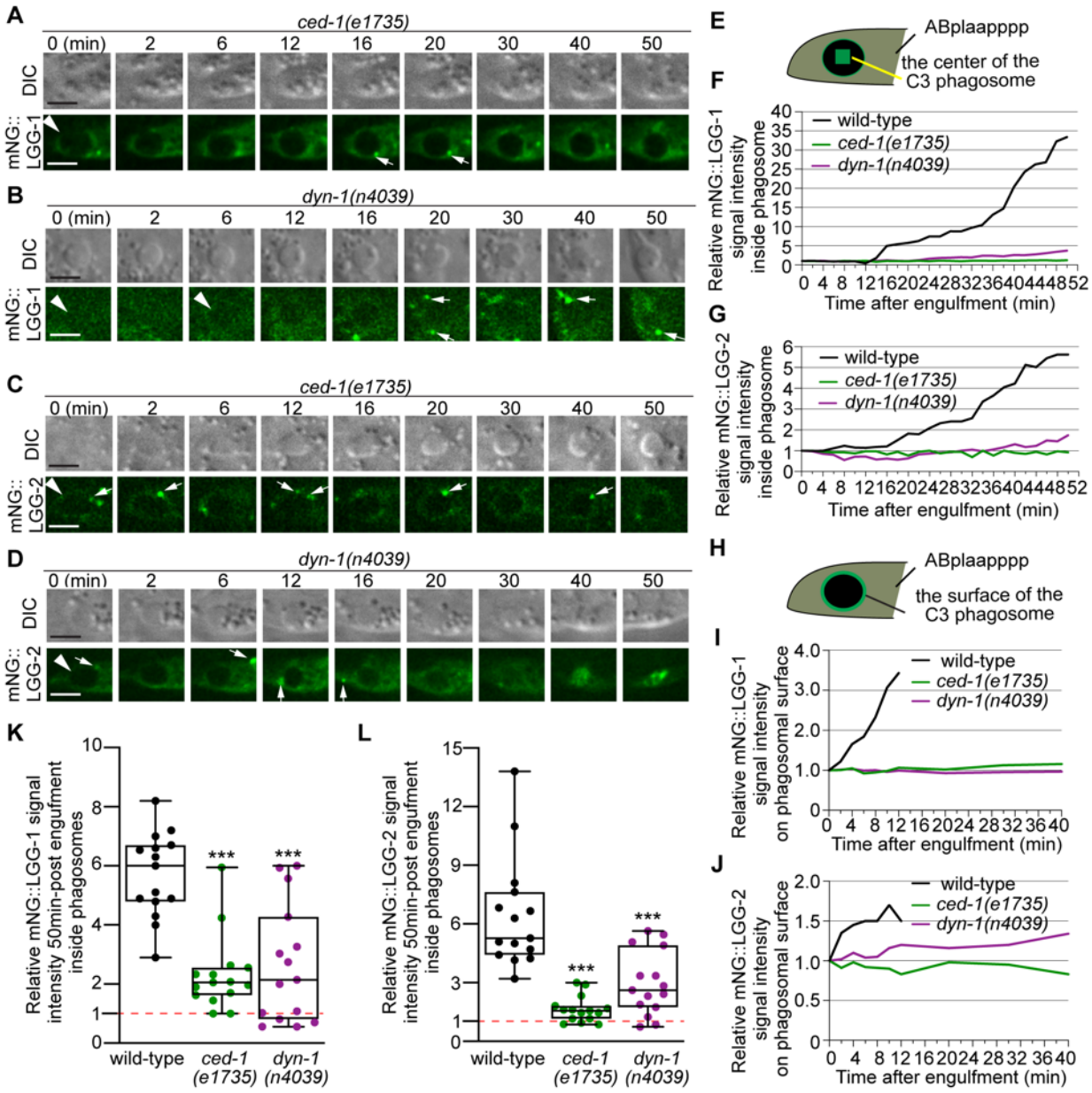

Figure 8. CED-1 and DYN-1 are essential for the incorporation of autophagosomes into phagosomes

(A-D) Time-lapse image series monitoring the presence or absence of puncta (white arrows) labeled with mNG::LGG-1 (A-B) or -2 (C-D) on C3 phagosomes (white arrowheads) and the subsequent entry of the mNG signal into the lumen in *ced-1* and *dyn-1* mutant embryos. DIC images mark the position of the cell corpse. “0 min” is the moment when phagosomes are just sealed. Scale bars are 2μm.

(E) A diagram illustrating that the relative mNG signal in the center of a phagosome is measured over time to create sub-figures (F) and (G). At time point t (time after “0 min”), the Relative Signal Intensity $_T$ = (Unit Intensity(phagosome center)$_T$ –Unit Intensity(background)$_T$) / (Unit Intensity(phagosome center)$_{T0}$- Unit Intensity (background)$_{T0}$).

528 (F-G) The relative mNG::LGG-1 (F) or -2 (G) signal intensity in the center of a phagosome (Y-axis) over
529 time in the 2-min interval (X-axis). “0 min” is the moment when pseudopods are sealed and a nascent
530 phagosome forms. (F) The data for the wild-type, *ced-1(e1735),* and *dyn-1(n4039)* mutant embryos are
531 from Figs 1F and 8(A-B), respectively. (G) The data for the wild-type, *ced-1(e1735),* and *dyn-1(n4039)*
532 mutant embryos are from Figures 1I and 8(C-D), respectively.
533 (H) A diagram illustrating that the relative mNG signal on the surface of a phagosome is measured over
534 time to create sub-figures (I) and (J). At time point T (time after “0” min), the Relative signal intensity $_T$
535 = (Unit Intensity(phagosome surface (the green ring))$_T$ –Unit Intensity(background)$_T$) / (Unit
536 Intensity(phagosome surface)$_{T0}$ - Unit Intensity (background)$_{T0}$).
537 (I-J) The relative mNG::LGG-1 or -2 signal intensity on the surface of a phagosome (Y-axis) over time
538 in the 2-min interval (X-axis). “0 min” indicates the moment when pseudopods are sealed and nascent
539 phagosome forms. (I) The data for the wild-type, *ced-1(e1735),* and *dyn-1(n4039)* mutant embryos are
540 from Figures 1F and 8(A-B), respectively. (J) The data for the wild-type, *ced-1(e1735),* and *dyn-*
541 *1(n4039)* mutant embryos are from Figs 1I and 8(C-D), respectively.
542 (K-L) Box-and-Whiskers plots of the relative mNG signal intensity measured in the center of
543 phagosomes 50 min-post the formation of nascent C3 phagosomes from 15 each of wild-type, *ced-*
544 *1(e1735),* and *dyn-1(n4039)* mutant embryos. Red dashed lines indicate the position of value 1, which
545 represents no signal enrichment relative to the background signal. ***, $p<0.001$, Student *t*-test of each
546 mutant compared to the wild-type value.
547

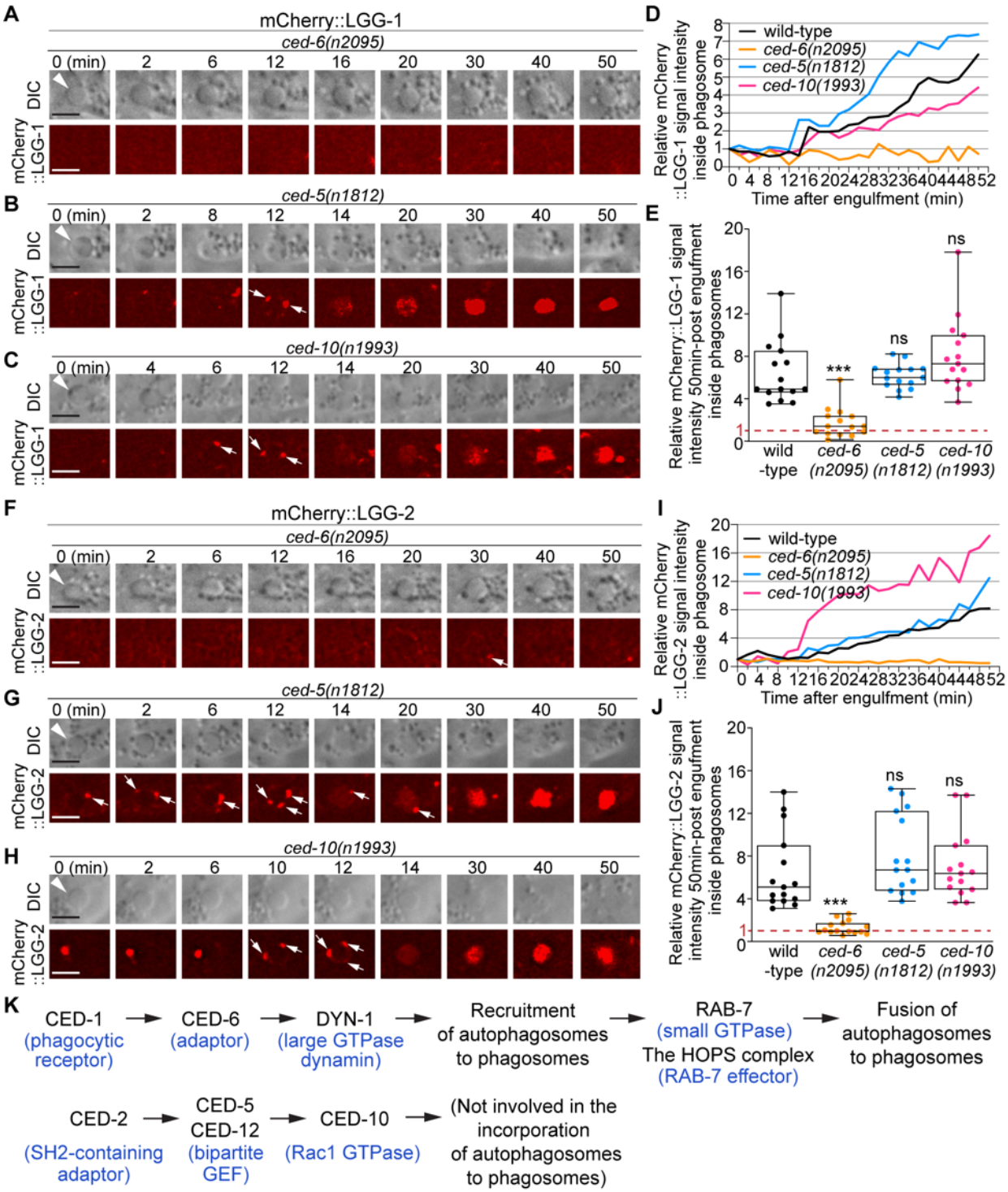

Figure 9. *ced-6*, but not *ced-5* or *ced-10,* is required for the incorporation of autophagosomes into phagosomes

(A-C and F-H) Time-lapse image series monitoring the presence or absence of puncta (white arrows) labeled with mCherry::LGG-1 (A-C) or -2 (F-H) on C3 phagosomes (white arrowheads) and the subsequent entry of the mCherry signal into the phagosomal lumen in *ced-6, ced-5,* and *ced-10* mutant

554 embryos. DIC images mark the position of the cell corpse. “0 min” is the moment when a nascent
555 phagosome just seals. Scale bars are 2μm.
556 (D and I) The relative mCherry::LGG-1 (D) or -2 (I) signal intensity in the center of a phagosome (Y-
557 axis) over time (in the 2-min interval) (X-axis). “0 min” indicates the moment when a nascent
558 phagosome just seals. (D) The data for the wild-type, *ced-6(n2095), ced-5(n1812),* and *ced-10(n1993)*
559 mutant embryos are from Figs 1E and 9(A-C), respectively. (I) The data for the wild-type, *ced-*
560 *6(n2095), ced-5(n1812),* and *ced-10(n1993)* mutant embryos are from Figs 1H and 9(F-H),
561 respectively.
562 (E and J) Box-and-Whiskers plots of the relative mCherry signal intensity measured in the center of
563 phagosomes 50 min-post the formation of nascent C3 phagosomes from 15 each of wild-type, *ced-*
564 *6(n2095), ced-5(n1812),* and *ced-10(n1993)* mutant embryos. The Red dashed lines indicate where
565 value 1, which represents no signal enrichment relative to the background signal, stand. “***”, $p<0.001$;
566 ns, not significant, Student *t*-test against the wild-type samples.
567 (K) A diagram illustrating that between the two parallel pathways that regulate the clearance of
568 apoptotic cells, only the CED-1 pathway, but not the other pathway, plays an essential role in promoting
569 the incorporation of autophagosomes into phagosomes. Blue letters in parentheses are the names of
570 the mammalian homolog of the corresponding *C. elegans* proteins.
571

572 **The incorporation of lysosomes into phagosomes is not affected by the lack of autophagosomes**

573 The incorporation of lysosomes to phagosomes is an essential force that drives the degradation of
574 phagosomal contents [3]. Because a portion of the autophagosomes would fuse with lysosomes and
575 become autolysosomes that retain lysosomal features [9], it is possible that the LGG^+ particles, which
576 include both autophagosomes and autolysosomes, might act to provide additional vesicles bearing
577 lysosomal features (such as autolysosomes) to the phagosomes. To test whether this is the case, we
578 examined whether mutations that specifically impair autophagosomes biogenesis would affect the
579 amount of organelles with lysosomal features, including lysosomes and autolysosomes that are
580 incorporated into phagosomes, and the temporal dynamics of the incorporation. *C. elegans* NUC-1 is an
581 endonuclease belonging to the DNase II family and resides in the lysosomal lumen [43,44]. We used a
582 *nuc-1::mCherry* reporter expressed in engulfing cells to quantify the rate of lysosome-phagosome
583 fusion. In time-lapse recording images monitoring phagosomes containing cell corpses C1, C2, and C3
584 in wild-type embryos, we observed the attachment of NUC-1::mCherry puncta on the surfaces of
585 phagosomes and the subsequent accumulation of the mCherry signal into the phagosomal lumen (**Fig**
586 **10A**). This dynamic process represents the recruitment and the subsequent fusion of lysosomal particles
587 to phagosomes and the delivery of NUC-1::mCherry into the phagosomal lumen. We next measured the

588 signal level of NUC-1::mCherry in the center of phagosomes in *lgg-1(tm3489)*, *lgg-2(tm5755)*, and *atg-*
589 *7(bp411)* embryos over time and observed accumulation of mCherry signal in the phagosomal lumen in
590 all samples (**Fig 10 A-E**). These three mutants are defective in the biogenesis of autophagosomes.
591 Quantitative analysis of 15 phagosomes of each genotype found that, 60 min after the formation of the
592 nascent phagosomes, (1) no significant difference in the mCherry signal level in the phagosomal lumen
593 in *lgg-2* mutants compared to wild-type samples (**Fig 10F**), and (2) slight elevation of the mCherry
594 signal in the lumen of *lgg-1* and *atg-7* mutant samples. In addition, the median value of the first time
595 point when NUC-1::mCherry signal was detected inside the phagosomal lumen was not significantly
596 different in all four genotypes (**Fig 10G**). All these data demonstrate that the incorporation of
597 lysosomes into phagosomes in *lgg-1*, *lgg-2*, and *atg-7* mutants is at least as efficient as in wild-type
598 embryos. Therefore, defects in the formation of autophagosomes, which potentially would result in the
599 lack of autolysosomes, do not affect the incorporation of lysosomes into phagosomes.
600

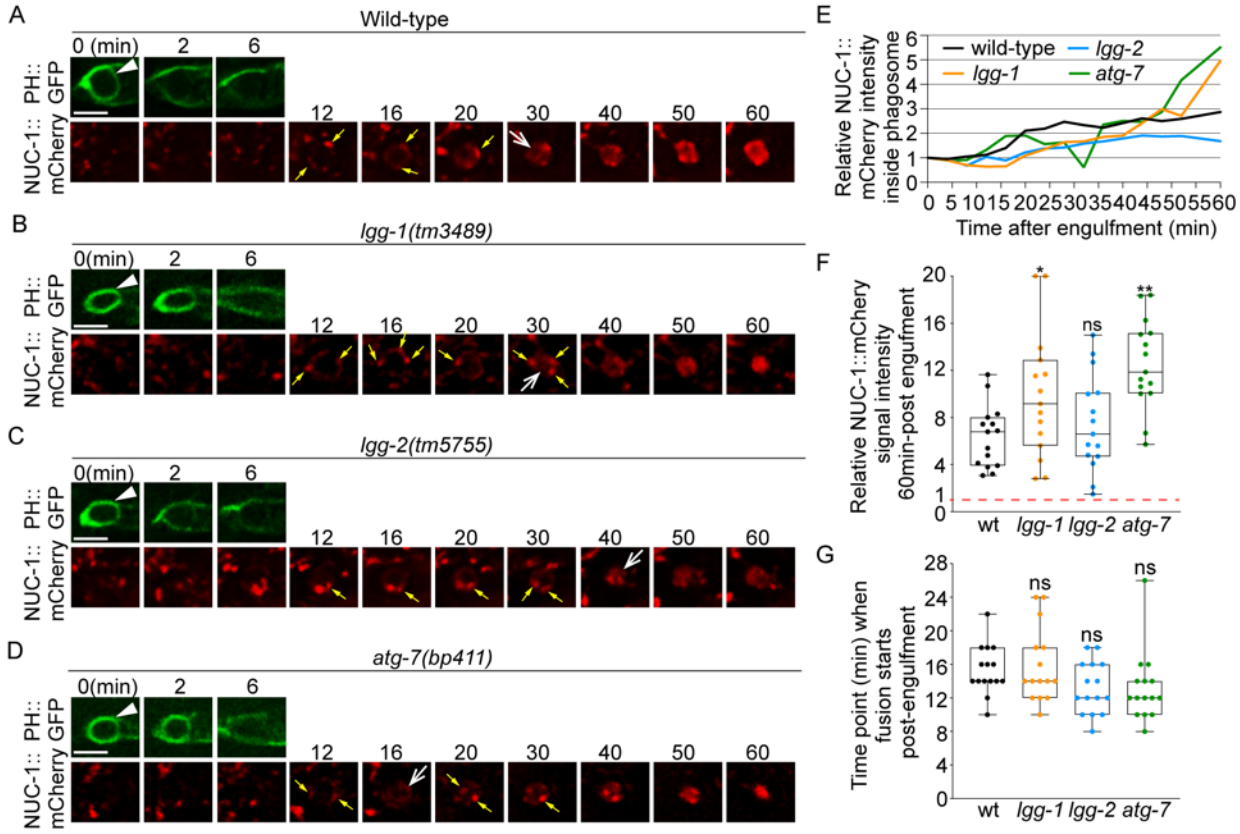

601

602 **Figure 10. Defects in the formation of autophagosomes do not affect the timing or efficiency of**
603 **lysosomes incorporation into phagosomes**
604 The time-lapse recording was conducted on phagosomes containing C1, C2, and C3 in wild-type and
605 named mutant embryos carrying $P_{ced\text{-}1}$*nuc-1::mCherry*, the lysosomal lumen reporter, and $P_{ced\text{-}}$

606 *$_1$PH(PLCγ)::gfp*, the marker for extending pseudopods and nascent phagosomes. (A-D) Fluorescence
607 time-lapse images of one C3 phagosome in each strain with the indicated genotype. "0 min" is the
608 moment when a nascent phagosome (white arrowhead) just seals. Yellow arrows mark the lysosomal
609 particles that are located on phagosomal surfaces. White open arrows mark the phagosomes with
610 mCherry signals in the lumen. Scale bars are 2.5 μm.
611 (E) The relative NUC-1::mCherry signal intensity in the center of a phagosome (Y-axis) over time (in 2-
612 min interval) (X-axis). "0 min" indicates the moment when a nascent phagosome is just sealed. Data
613 are from Fig 10 (A-D).
614 (F) A Box-and-Whiskers graph of the relative mCherry signal intensity measured in the center of
615 phagosomal lumen 60 min-post the formation of nascent C3 phagosomes from 15 each of wild-type,
616 *lgg-1(tm3489), lgg-2(tm5755),* and *atg-7(bp411)* mutant embryos. A dashed red line marks the position
617 where the relative signal intensity value =1, which indicates no enrichment of mCherry signal inside the
618 phagosomal lumen.
619 (G) A Box-and-Whiskers graph displaying the first time point when the NUC-1::mCherry signal is
620 detected inside the lumen of 15 C3 phagosomes in wild-type, *lgg-1(tm3489), lgg-2(tm5755),* and *atg-*
621 *7(bp411)* mutant embryos.
622

623 ## Discussion

624 Autophagosomes play essential roles in cellular homeostasis by eliminating harmful protein
625 aggregates and damaged organelles, and in stress response by converting intracellular organelles to
626 nutrients during starvation [9]. We have identified a novel function of autophagosomes in facilitating
627 the degradation of apoptotic cells through fusing to phagosomes. In *C. elegans* cells that engulf
628 apoptotic cells, autophagosomes are recruited to the surfaces of phagosomes and subsequently fuse to
629 the phagosomal membrane. Through this previously unknown interaction, autophagosomes release
630 substances to the phagosomal lumen and membrane. We have further identified a signaling pathway
631 that promotes the recruitment and subsequent fusion of autophagosomes to phagosomes. Together,
632 these findings reveal a novel mechanism through which the pathways that control autophagy and
633 phagocytosis converge, underlining the importance of this mechanism in the degradation of apoptotic
634 cells. We propose that this mechanism might be conserved in the metazoans and has important impact
635 in the regulation of the immunological consequences of dying cells inside human bodies.
636

637 **Canonical autophagosomes play an essential role in the degradation of apoptotic cells**

638 Previously, *C. elegans* autophagy genes have been implicated in facilitating the clearance of
639 apoptotic cells. Autophagy occurring in apoptotic cells was proposed to facilitate the exposure of
640 phosphatidylserine, which is the "eat me" signal that attracts engulfing cells to the surfaces of apoptotic
641 cells in mice embryonic bodies and *C. elegans* [45,46]. Multiple autophagy genes were reported to
642 participate in the clearance of apoptotic cells in *C. elegans* engulfing cells [11-13,46]. They were
643 reported to work together with Class II PtdIns3 kinase PIKI-1 to facilitate the production of PtdIns(3)P
644 on phagosomal surfaces [11], to promote the recruitment of RAB-5 and RAB-7 to the phagosomal
645 surfaces [13], and to promote phagosome degradation [46]. The above reports suggest that the
646 autophagy genes examined might have separate functions in the degradation of phagosomal contents not
647 related to their canonical roles in autophagosome biogenesis. Our work reported here, on the other
648 hand, presents a different discovery regarding how the autophagy machinery regulates phagosome
649 degradation.
650 We found that the canonical double-membrane autophagosomes actively participate in the
651 degradation of apoptotic cells inside phagosomes. Four critical sets of evidence indicate that the LGG-
652 1- and -2-labeled vesicles that are incorporated into phagosomes are autophagosomes, not the single-
653 membrane LAP vesicles. First, the membrane-bound LGG-1 or -2 reporters were observed to enter the
654 phagosomal lumen after vesicle-phagosome fusion. Only when the vesicles are composed of double
655 membranes and when the reporter molecules label both the inside and outside membranes, the entry of
656 the signal into phagosomal lumen is possible (**Fig 1K**). Conversely, if the LGG-1 or -2 labeled vesicles
657 are of a single membrane, after vesicle-phagosome fusion, the reporter signal would remain on the
658 phagosomal membrane, as the membrane-bound lysosomal marker CTNS-1::mRFP does (**Fig S1**).
659 Secondly, these vesicles are also labeled with GFP-tagged ATG-9, an integral membrane protein
660 inserted into the autophagosomal membranes. Thirdly, the production of these vesicles relies on genes
661 pivotal for autophagosome biogenesis, such as *atg-3*, *atg-7*, and *atg-9*. Last but not least, genes
662 encoding the *C. elegans* homologs of mammalian ULK1, ATG13, and ATG14, which are dispensable
663 for the generation of LAP vesicles in mammalian cells [6], are required for the formation of the LGG-
664 labeled vesicles discussed here and for the efficient clearance of apoptotic cells, further verifying that
665 these vesicles are distinct from the single-membrane LAP vesicles. Together, these four sets of findings
666 demonstrate that double-membrane autophagosomes, not single-membrane LAP vesicles, are being
667 incorporated into phagosomes.
668 In *C. elegans*, LC3-dependent phagocytosis was reported to function in the clearance of the
669 midbody, a structure that is essential for the completion of cytokinesis, and the second polar body

670 generated during female meiosis [47,48]. The clearance of midbodies and second polar body is
671 considered independent of autophagosomes based on the observation that neither *unc-51* nor *epg-8* is
672 required for the above processes [47,48]. However, since whether the LGG markers attached to
673 phagosomes carrying midbodies or polar bodies represent double-membrane or single-membrane
674 vesicles have not been investigated [47,48], whether LAP vesicles exist in *C. elegans* cells still needs to
675 be demonstrated.
676 The observation of the LGG-1 or -2 signals inside the phagosomal lumen is shown through the
677 presence of mCherry as a reporter molecule. The mCherry protein is resistant to acidic pH [30].
678 Phagosome luminal pH value reduces from 5.5-6.0 to 4.5-5.5 after incorporating lysosomes [49], leading
679 to the inactivation of the fluorophore in the commonly used GFP reporter [29]. In fact, in *C. elegans*
680 engulfing cells, GFP-tagged LGG-1 or -2, unlike the mCherry-tagged reporters, are only observed on the
681 surfaces but not in the lumen of phagosomes, presumably due to the acidic environment of the
682 phagosomal lumen (**Fig 1**). It is thus conceivable that in other experimental systems, a mCherry-tagged
683 LC3 marker might disclose a previously overlooked fusion between autophagosomes and phagosomes.
684 Based on the evolutionary conservation of almost all molecular mechanisms, in particular the
685 strong conservation of the known mechanisms that control phagocytosis and autophagy in metazoans
686 [25,34], we propose that in in mammalian cells, besides LAP vesicles, canonical autophagosomes might
687 also contribute to the degradation of apoptotic cells in phagosomes. The demonstration of an
688 autophagosome-phagosome fusion event in *C. elegans*, a well-established model organism for the study
689 of cell death-related events, opens a path to investigate whether the event and mechanism of
690 autophagosome-phagosome fusion is an evolutionarily conserved event. In addition, the
691 autophagosome-phagosome fusion might contribute to the degradation of other kinds of phagosomal
692 cargos besides apoptotic cells.
693
694 **LGG-1 and LGG-2 define three subpopulations of autophagosomes that are incorporated into**
695 **phagosomes**
696 LGG-1 and -2 are close homologs that each labels autophagosomes. We have observed three
697 separate classes of autophagosomes that are incorporated into phagosomes: LGG-1^{+} LGG-2^{-}, LGG-1^{-}
698 LGG-2^{+}, or LGG-1^{+} LGG-2^{+}. These subpopulations might represent autophagosomes at different stages
699 of maturation [26]. Remarkably, we have found that the *lgg-1*; *lgg-2* double mutants display a much
700 enhanced Ced phenotype than that displayed by each of the *lgg-1* or *lgg-2* single mutants. Together,
701 these results indicate that autophagosomes at different stages of maturity all contribute to the

702 degradation of apoptotic cells. These results are also consistent with our finding that the
703 autophagosomes-phagosome fusion is independent of lysosome-phagosome fusion (**Fig 9**).
704
705
706 **What do autophagosomes contribute to the degradation of apoptotic cells**
707 We have found that the blockage of the biogenesis of autophagosomes or the recruitment of
708 autophagosomes to phagosomes result in a significant delay in the degradation of phagosomal content
709 and, consequently, the persistent appearance of engulfed cell corpses. The incorporation of
710 autophagosomes into phagosomes presumably delivers certain substances to the lumen and/or
711 membrane of phagosomes, substances that are important for the degradation of phagosomal contents.
712 Currently, the identities of these substances are still a mystery. Studies in mammalian cells implicate
713 LAP vesicles in facilitating the incorporation of lysosomes into phagosomes [5,6]. In *C. elegans*
714 mutants defective for the biogenesis of autophagosomes (*atg-7*, *lgg-1*, and *lgg-2* mutants), we found that
715 the lack of autophagosomes does not affect the efficiency of lysosome-phagosome fusion (**Fig 10**). This
716 result, together with the observation that the three subpopulations of autophagosomes at different
717 maturation stages all fuse to phagosomes, suggests that it is not just the sub-population of
718 autolysosomes, which have lysosomal features, that contribute to phagosomal degradation. Thus
719 autophagosomes might deliver something unique to the phagosome, something not present in lysosomes
720 or endosomes. These substances also might not be limited to proteins in the autophagosome lumen or
721 membranes; they could be specific lipid molecules from the membranes of autophagosomes. Further
722 investigation is required to discover the identities of this (these) molecule(s).
723
724 **The CED-1 signaling pathway drives the incorporation of autophagosomes to phagosomes**
725 Autophagosomes are incorporated into phagosomes in two sequential steps: (1) they are recruited
726 to the surfaces of phagosomes, detected by the enrichment of punctated LGG-1 or -2 fluorescence
727 reporters on phagosomal surfaces, and (2), they subsequently fuse to phagosomes, detected by the
728 enrichment of the LGG-1 or -2 reporter signals inside the phagosomal lumen. RAB-7 and its effector,
729 the HOPS complex, are known to act as tethering factors that facilitate the fusion of various intracellular
730 organelles, including autophagosomes, to lysosomes [26,50]. Closely related to this study, RAB-7 and
731 VPS-18 are pivotal for the fusion between lysosomes and phagosomes and for the degradation of
732 apoptotic cells inside phagosomes in *C. elegans* [19,42,51]. Here we have discovered that RAB-7 and
733 VPS-18 play essential and specific roles in the fusion but not for the recruitment of autophagosomes to

734 phagosomes. Our finding adds a new pair of organelles that depend on the RAB-7/HOPS complex for
735 fusion to each other. As RAB-7 is enriched on the surfaces of both phagosomes and autophagosomes
736 ([19] and (**Fig 7(B-D)**), and as the HOPS complexes in mammalian cells and Drosophila are known to
737 interact with the SNARE complex, the membrane fusion machinery [52,53], we propose that the RAB-
738 7/HOPS complex acts on the surfaces of phagosomes and autophagosomes to facilitate autophagosomes-
739 phagosome fusion via promoting the interaction between the SNARE complexes on phagosomes and
740 autophagosomes (**Fig 7I**). Currently, the specific SNARE proteins that catalyze the autophagosomes-
741 phagosome fusion have not been identified.
742 The CED-1 signaling pathway, which initiates the maturation of phagosomes that bear apoptotic
743 cells, is essential for the enrichment of GTP-bound RAB-7 to the surfaces of phagosomes [19]. Here we
744 have found that CED-1, CED-6, and DYN-1 drive the incorporation of autophagosomes to phagosomes,
745 in addition to driving the incorporation of early endosomes and lysosomes previously discovered
746 [19,21]. In *ced-1* mutants, for example, the recruitment of autophagosomes to the surfaces of
747 phagosomes is almost completely blocked. Due to the severe recruitment defect, whether the *ced-1* null
748 mutation further impairs the fusion between autophagosomes and phagosomes cannot be readily
749 visualized. However, since a *ced-1* null mutation impairs the recruitment of RAB-7 to [19] and the
750 production of PtdIns(3)P on phagosomal surfaces [19,23], and since the recruitment of the HOPS
751 complex to the surfaces of intracellular organelles requires both RAB7 and PtdIns(3)P [39,54,55], we
752 predict that the CED-1 pathway would also control the RAB-7/HOPS complex-mediated
753 autophagosomes-phagosome fusion (**Fig 9K**). Identifying the CED-1 signaling pathway as the driving
754 force for the incorporation of autophagosomes to phagosomes helps to reveal the molecular mechanisms
755 behind the crosstalk between autophagy and phagocytosis.
756

757 ## Materials and Methods

758 **Mutations, strains, and transgenic arrays**

759 *C. elegans* strains were grown at 20ºC as previously described [56] unless indicated otherwise.
760 The N2 Bristol strain was used as the wild-type control strain. Mutations are described in [57] and by
761 the Wormbase (http://www.wormbase.org) unless noted otherwise (**Table S1**): LG1: *ced-1(e1735), epg-*
762 *8(bp251)*; LGII: *lgg-1(tm3489), rab-7(ok511), vps-18(tm1126)*; LGIII: *atg-13(bp414), ced-6(n2095);*
763 LGIV: *atg-3(bp412), atg-7(bp411), ced-5(n1812), ced-10(n1993), lgg-2(tm5755* and *tm6474)*; LGV:
764 *atg-9(bp564), atg-18(gk378), unc-76(e911), unc-51(e369)*; LGX: *atg-2(bp576), dyn-1(n4039). dyn-*
765 *1(n4039)* homozygous mutants, which are zygotic embryonic lethal, were maintained by an

766 extrachromosomal array carrying a wild-type *dyn-1* gene and a co-expressed P_{egl-13}*gfp* marker (**Table**
767 **S1**) [21]. *dyn-1(n4039)* homozygous embryos losing the rescuing transgene were identified as the
768 embryos not carrying P_{egl-13}*gfp*. The *rab-7(ok511) and lgg-1(tm3489)* homozygous strains are both
769 maternal-effect embryonic lethal, and the mIn1 balancer maintained each allele with an integrated
770 pharyngeal GFP marker (**Table S1**) [58]. To obtain *rab-7(ok511)* m^-z^- homozygous embryos, GFP^- *rab-*
771 *7(ok511)* homozygous hermaphrodites were isolated among the progeny of the strain VC308, and their
772 progeny were collected as embryos. The same protocol was used to collect *lgg-1(tm3489)* m^-z^- embryos
773 from the strain GK738 (**Table S1**). Double mutants between *lgg-1(tm3489)/mIn1* and *lgg-2(tm6474)*
774 were generated by standard genetic crosses.
775 Extrachromosomal arrays were generated by the microinjection of plasmids with the co-injection
776 marker p76-18B [*punc-76(+)*] into *unc-76(e911)* mutants [59,60]. Non-Unc mutants were identified as
777 transgenic animals. Integrated transgenic arrays were generated by gamma irradiation [60]. Integrated
778 arrays generated in this study are as follows (**Table S1**): LGI: *enIs87[*P_{ced-1}*PH(hPLCγ)::mrfp* and P_{ced-}
779 $_{1}$*mNG::lgg-1];* LGII: *enIs82[*P_{ced-1} *ced-1::gfp* and P_{ced-1} *mCherry::lgg-1];* LGV: *enIs85[*P_{ced-1}
780 *PH(hPLCγ)::mrfp* and P_{ced-1} *mNG::lgg-2];* LGX: *enIs83[*P_{ced-1} *ced-1::gfp* and P_{ced-1} *mCherry::lgg-2].*
781
782 **Plasmid construction**
783 *lgg-1* and *lgg-2* cDNAs were PCR amplified from a mixed-stage *C. elegans* cDNA library [61].
784 To generate the P_{ced-1} *gfp::lgg*-1 and P_{ced-1} *gfp::lgg-2* plasmids, *lgg-1* and *lgg-2* cDNAs were cloned into
785 the XmaI and KpnI sites of plasmid pZZ956 (*P_{ced-1} 5'gfp)* [61]. P_{ced-1} *mCherry::lgg-1 or -2* were
786 constructed by replacing the cDNA of *gfp* with that of mCherry [30]. P_{ced-1} *mNG (mNeonGreen)::lgg-1*
787 *or -2* were constructed by replacing the cDNA of *gfp* with that of mNeonGreen [62]. To generate P_{ced-}
788 $_{1}$*gfp::lgg-1(G116A)* and P_{ced-1}*gfp::lgg-2(G130A),* the QuickChange Site-directed Mutagenesis Kit
789 (Stratagene, La Jolla, CA) was used to introducing the above mutations into the constructs. To construct
790 P_{ced-1} *atg-9::mCherry, the atg-9a* open reading frame was PCR-amplified from a *C. elegans* mixed-stage
791 cDNA library and inserted between P_{ced-1} and *gfp* in pZZ829 (P_{ced-1} *3'gfp*) [61]. The *gfp* cDNA was then
792 replaced by the *mCherry* cDNA [30]. All plasmids contain an *unc-54* 3' UTR.
793
794 **Quantification of the number of cell corpses using Nomarski DIC microscopy**
795 Cell corpses display a highly refractive button-like morphology under Differential Interference
796 Contrast (DIC) microscopy. An Axionplan 2 compound microscope (Carl Zeiss, Thornwood, NY)
797 equipped with Nomarski DIC optics, an AxioCam digital camera, and AxioVision imaging software was

798 used for DIC microscopy. Using a previously established protocol [27], we quantified the number of
799 cell corpses in the head region at the 1.5-fold and 2-fold stage embryos, which are ~420 and ~460 min
800 post-first cleavage.
801
802 **Fluorescence microscopy and time-lapse imaging**
803 A DeltaVision Elite Deconvolution Imaging System (GE Healthcare, Inc.) equipped with a DIC
804 imaging apparatus and a Photometrics Coolsnap 2 digital camera was used to capture fluorescence, and
805 DIC images Applied Precision SoftWoRx 5.5 software was utilized for deconvolving and analyzing the
806 images [27]. To observe the amount of autophagosomes in ventral hypodermal cells that express P_{ced-1},
807 fourteen serial Z-sections in 0.5□l interval between adjacent optical sections, starting at the ventral
808 surface of embryos at mid-embryonic stages, were collected. The 2D projection image of each Z-stack
809 was generated and compared among different genetic backgrounds (**Figs S1**, **S2**, **S4**, and **S6**). To track
810 fluorescence markers on pseudopods, on the surfaces of phagosomes, or inside phagosomal lumen
811 during the clearance process of cell corpses C1, C2, and C3, embryos were monitored on their ventral
812 surface starting at ~310 min post-first cleavage using an established time-lapse imaging protocol [27].
813 Twelve to 16 serial *Z*-sections (at 0.5-μm intervals) were captured every 2 min, with recordings typically
814 lasting between 60 to 180 min. Embryos that exhibited normal elongation and movement were
815 considered developing properly. The moment engulfment starts is defined as when the extension of
816 pseudopods around C1, C2, or C3 is first observed. The moment a nascent phagosome form is defined
817 as when the pseudopods around a cell corpse join and make a full closure. The life span of a phagosome
818 is defined as the time interval between the moments when the nascent phagosome forms and when the
819 phagosome shrinks to one-half of its original diameter.
820 The time spans of the engulfment and degradation processes of cell corpses C1, C2, or C3 were
821 measured as previously established [61]. Briefly, a pseudopod marker, either CED-1::GFP or
822 PH(PLCγ)::GFP, was monitored over time. The moment engulfment starts is defined as when the
823 budding pseudopods around C1, C2, or C3 is first observed. The moment a nascent phagosome form is
824 defined as the moment when the pseudopods around a cell corpse join and make a full closure. The
825 period between the budding and the sealing of the pseudopods is the time span of engulfment. To
826 measure phagosome duration, a co-expressed phagosomal surface marker mCherry::2xFYVE was used
827 to track the diameter of the phagosome over time. The life span of a phagosome is defined as the time
828 interval between the time points when a nascent phagosome was born and when the phagosome shrank
829 to one-half of its original diameter.

830

831 **Quantitative measurement of signal intensity**

832 *Measuring the signal intensity inside the phagosomal lumen*

833 In embryos expressing mCherry- or mNG-tagged LGG-1 or LGG-2, to measure the fluorescence
834 signal intensity inside the phagosomal lumen over time, we identified the boundary of a phagosome and
835 the "0 min" time point when a nascent phagosome was formed by observing the co-expressed marker for
836 a nascent phagosome such as CED-1::GFP or PH(PLCγ)::GFP. At each time point, the total LGG-1 or -
837 2 image intensity of a fixed area (4x4 pixels) at the center of a phagosome ($Int_{phagosome}$) was recorded
838 (**Fig 1C**), so was the intensity of an area of the same size (4x4 pixels) outside the embryo as the
839 background image intensity ($Int_{background}$). The Relative image intensity (RInt) at a particular time point
840 (Tn) comparing to the start point (T0) is calculated as $RInt_{Tn} = (Int_{phagosome}-Int_{background})_{Tn} / (Int_{phagosome}-$
841 $Int_{background})_{T0}$. The $RInt_{Tn}$ value of 1.0 indicates no entry of LGG-1- or LGG-2-labeled autophagosomes
842 into the phagosomal lumen.

843 *Measuring the signal intensity on the surface of a phagosome*

844 To measure the efficiency of recruitment of autophagosomes to phagosomes, we quantified the
845 intensity of mCherry- or mNG-labeled LGG-1 or LGG-2 on the surfaces of phagosomes. First, we
846 identified the boundary of a phagosome and the "0 min" time point when a nascent phagosome just
847 formed by observing co-expressed CED-1::GFP or PH(PLCγ)::GFP. At a particular time point, Tn or
848 T0, the surface of a phagosome was outlined by two closed polygons (**Fig 8E**). The total signal
849 intensities, as well as the areas of the polygons, were recorded. The unit signal intensity of the "donut-
850 shape" area between the two polygons was calculated as follows:
851 Unit Intensity ($UI_{phagosome}$) = ($Intensity_{external\ polygon} - Intensity_{internal\ polygon}$)/($Area_{external\ polygon} - Area_{internal}$
852 $_{polygon}$). The Unit Background Intensity ($UI_{background}$) was measured from a polygon outside the embryo
853 was calculated as follow: $UI_{background} = Intensity_{background}/Area_{background}$.
854 At the time point Tn, the relative signal intensity ($RInt_{Tn}$) = $(UI_{phagosome} - UI_{background})_{Tn} / (UI_{phagosome} -$
855 $UI_{background})_{T0}$. The $RInt_{Tn}$ value 1.0 indicates no enrichment of LGG-1- or LGG-2-labeled
856 autophagosomes on phagosomal surfaces comparing to the "0 min" time point.

857

858

859 ## Acknowledgment

860 We thank Ying Wang for technical support and R. Haley for helpful comments. We thank the *C.*
861 *elegans* Genetics Center (CGC), funded by the NIH Office of Research Infrastructure Programs (P40

OD010440), for providing some strains. We also thank the National BioResource Project of Japan and Dr. Shohei Mitani for provides some strains.

Funding Source

NIH R01GM067848 supports this work.

Author Contributions

The authors have made the following declarations about their contributions: Conceived and designed the experiments: OPR ZZ. Performed the experiments: OPR LC XL TY HH ZZ. Analyzed the data: OPR TY ZZ. Prepare the manuscript: OPR ZZ.

Competing Interests

The authors declare no competing interests

876 Supplemental material

877

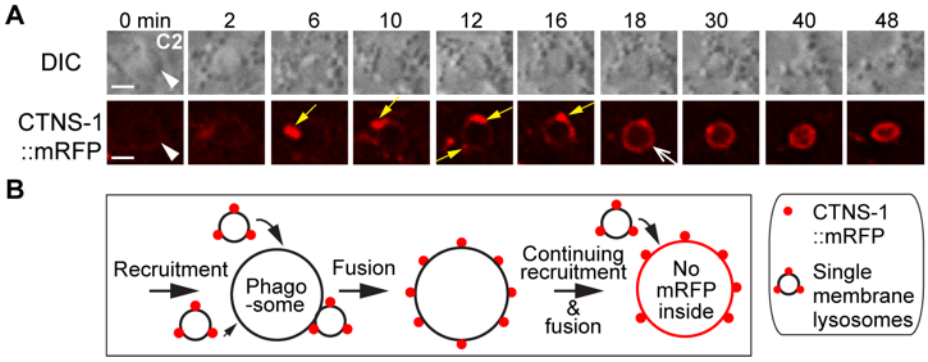

878

879

880 **Figure S1. The fusion of lysosomal particles to phagosomes results in the incorporation of**
881 **lysosomal membrane protein CTNS-1 to the phagosomal membrane but not the lumen**

882 (A) Time-lapse images of a C2 phagosome and the lysosomes that are recruited to and subsequently
883 fuse with it. CTNS-1::mRFP is expressed in engulfing cells under P_{ced-1}. "0 in" is the time point when a
884 C2 phagosome (white arrowheads) just forms. Yellow arrows mark CTNS-1::mRFP-labeled lysosomal
885 particles. One open white arrow marks the phagosomal surface that is evenly colored by mRFP. Scale
886 bars are 2μm.

887 (B) A diagram illustrating that the single membrane-vesicles that are labeled with CTNS-1::mRFP on
888 their membranes are recruited to phagosomal surfaces and fused to the phagosomal membrane. After
889 the fusion between the membranes of these vesicles and the phagosome, the mRFP signal is evenly
890 distributed to the phagosomal surface. However, no mRFP signal enters the phagosomal lumen.

891

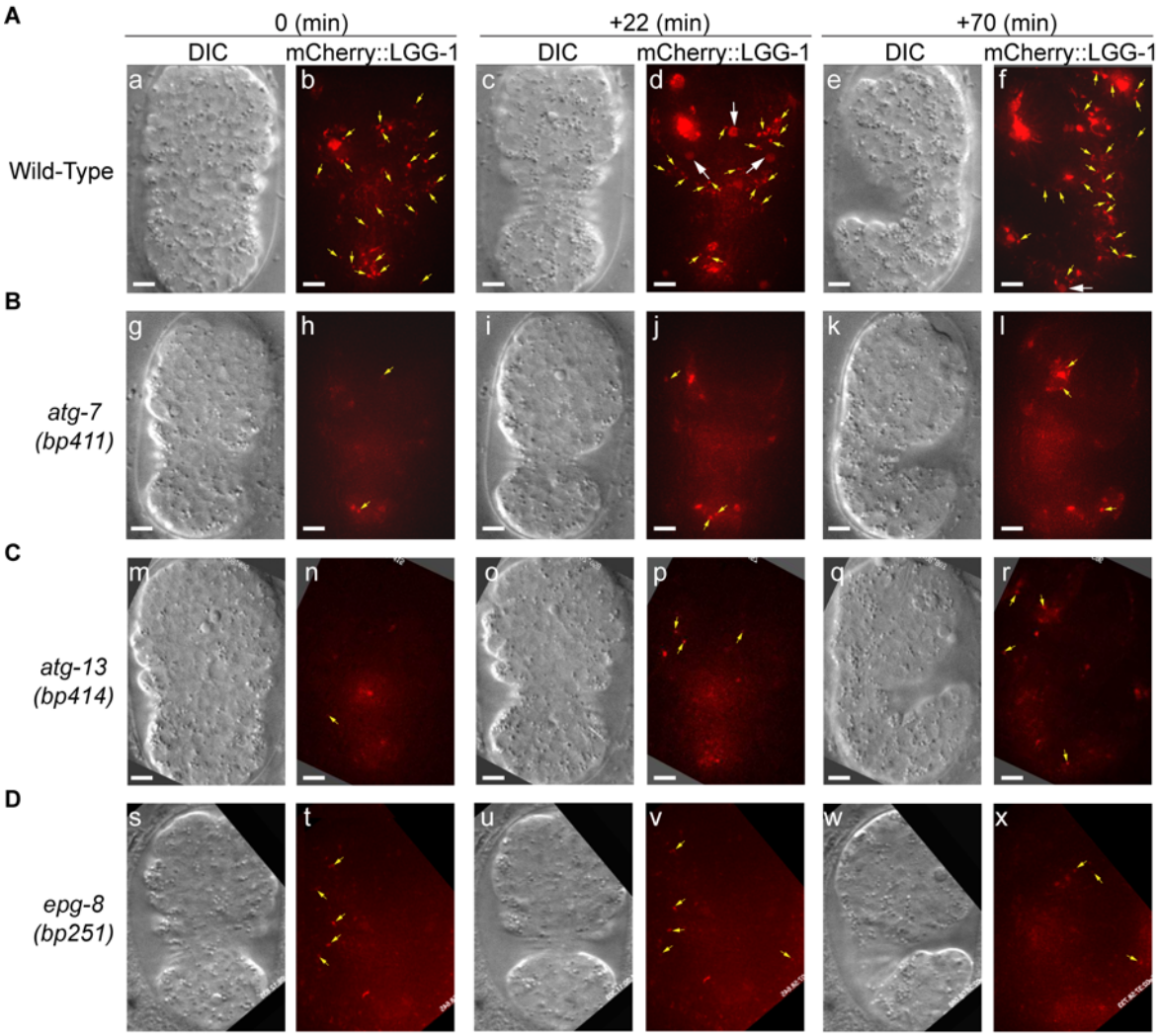

892
893
894 **Figure S2. The *atg-7*, *atg-13*, and *epg-8* mutants are severely defective in the production of LGG-**
895 **1-labeled autophagosomes**
896 Images of wild-type (A), *atg-7(bp411)* (B), *atg-13(bp414)* (C), and *epg-8(bp251)* mutant (D) embryos
897 expressing P_{ced-1} *mCherry::lgg-1* are presented. "0 min" labels embryos that are ~330 min post-1st
898 cleavage. The mCherry images are 2-D projections of 14 Z-sections at 0.5 µm intervals. Red puncta
899 (yellow arrows) represent autophagosomes. White arrows in (A(d)) mark three phagosomes, on the
900 surface of which mCherry signal is recruited in (a-b), and 20 min later, enters the phagosome,
901 demonstrating the autophagosomes/phagosome fusion event. Scale bars are 5 µm.
902

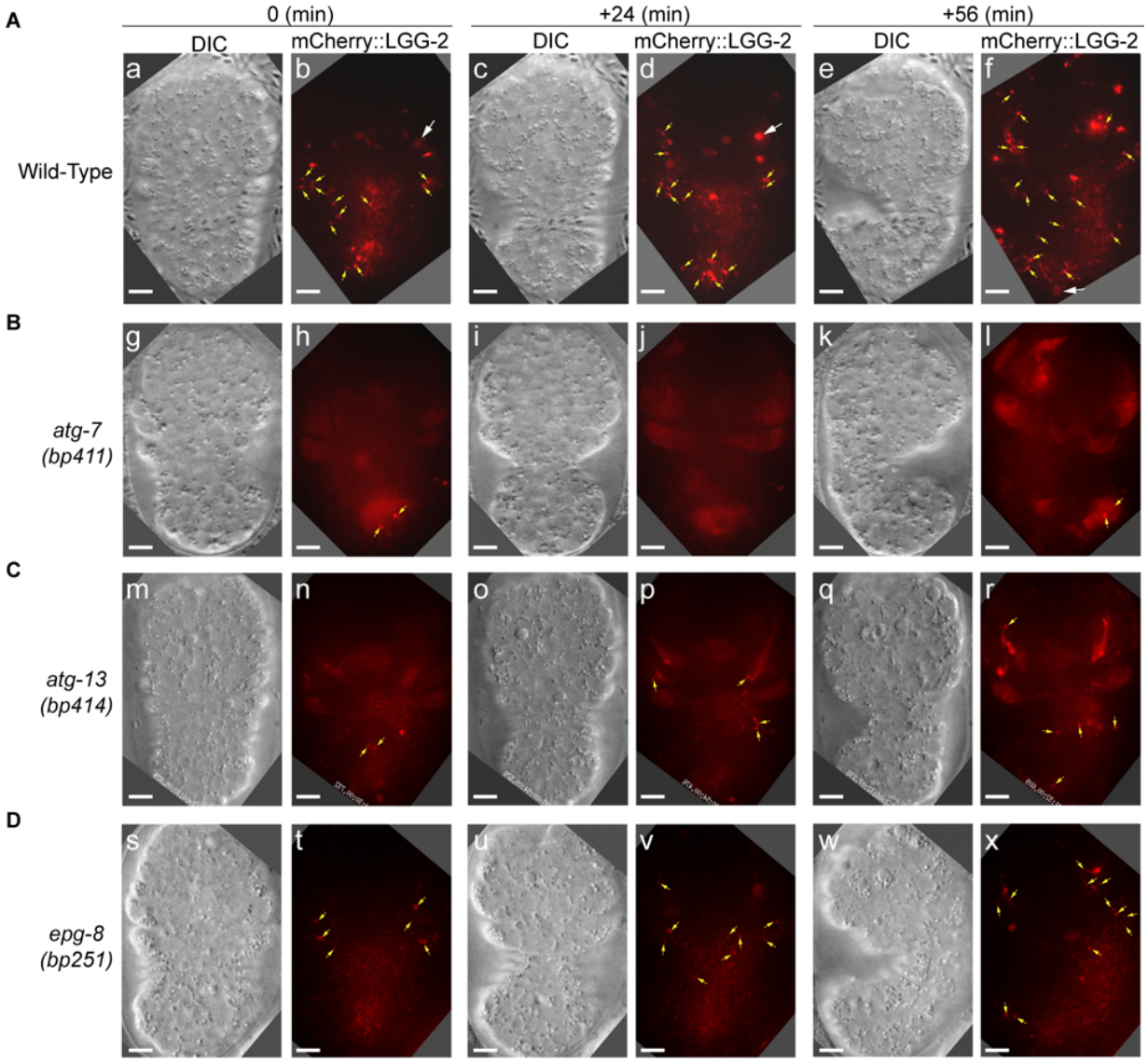

903
904

905 **Figure S3. The *atg-7*, *atg-13*, and *epg-8* mutants are severely defective in the production of LGG-**
906 **2-labeled autophagosomes**

907 Images of wild-type (A), *atg-7(bp411)* (B), *atg-13(bp414)* (C), and *epg-8(bp251)* mutant (D) embryos
908 expressing P_{ced-1} *mCherry::lgg-1* are presented. "0 min" labels embryos that are ~330 min post-1st
909 cleavage. The mCherry images are 2-D projections of 14 Z-sections at 0.5 µm intervals. Red puncta
910 (yellow arrows) represent autophagosomes. White arrows in (A(b, d)) mark one phagosome, on the
911 surface of which mCherry puncta are recruited to in (b), and 24 min later, mCherry enters the
912 phagosome, demonstrating the autophagosomes/phagosome fusion event. Scale bars are 5 µm.
913

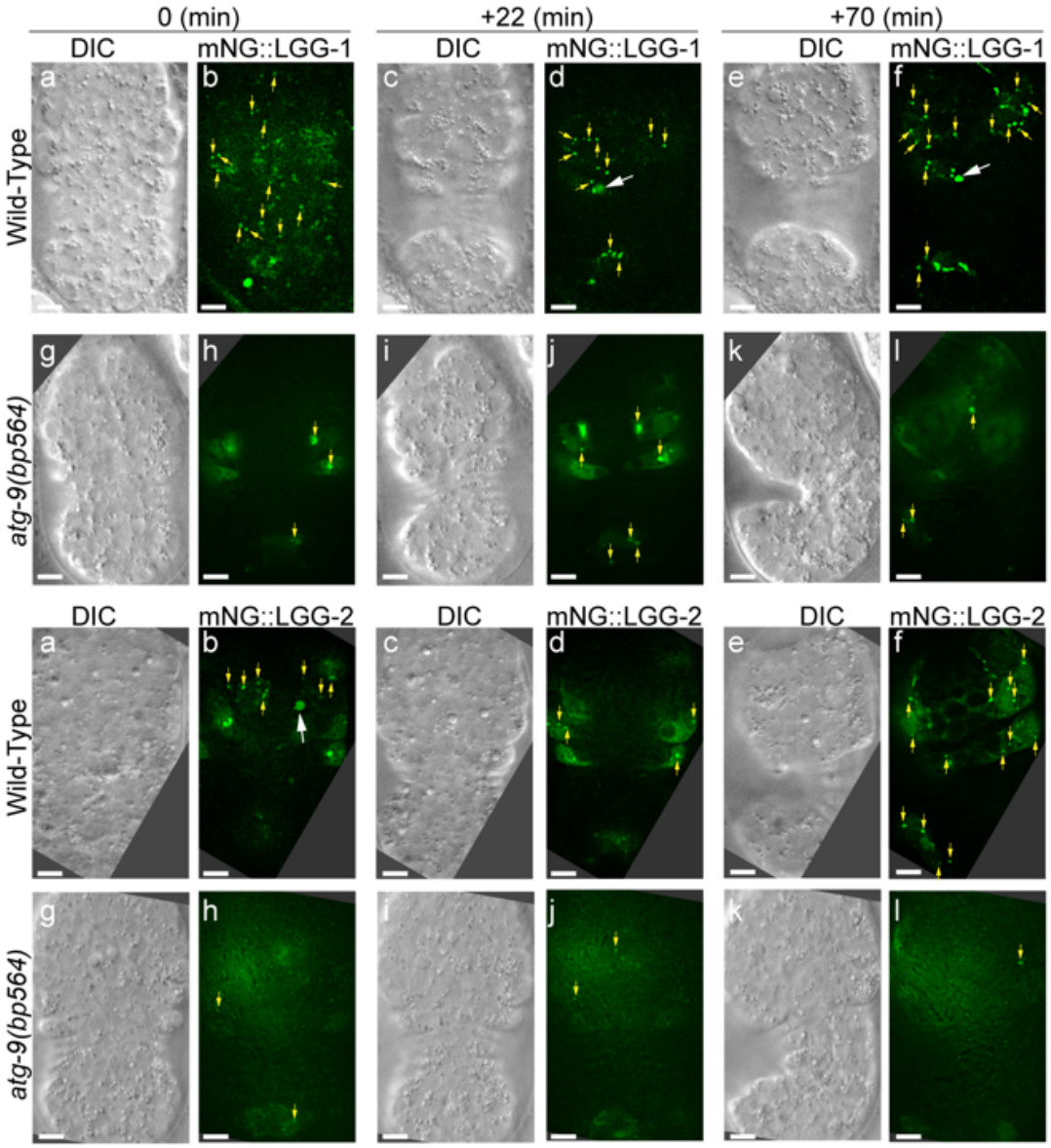

Figure S4. *atg-9* is another gene essential for the production of autophagosomes and the incorporation of autophagosomes into phagosomes

(A-B) Time-lapse image series monitoring the presence or absence of puncta labeled with mNG:: LGG-1 (A) or mNG::LGG-2 (B) on phagosomes (white arrowheads) and the subsequent entry of mCherry signal into the lumen in *atg-7* mutant embryos. DIC images mark the position of the cell corpse. "0 min": when engulfment is just completed (determined by PH::mCherry). Scale bars are 2μm. Yellow arrows mark mNG puncta located on the surfaces of phagosomes.

(C-D) Box-and-Whiskers plots of the relative mNG signal intensity measured in the center of phagosomes 60 min-post the formation of nascent C3 phagosomes from 15 each of wild-type and *atg-9(bp564)* mutant embryos.

926 (E-F) Images of wild-type and *atg-9(bp564)* mutant embryos expressing P_{ced-1} *mNG::lgg-1* (E) or *::lgg-2*
927 (F) are presented. “0 min” embryos are embryos at ~330 min post-1st cleavage. The mNG images are
928 2-D projections of 14 Z-sections at 0.5 µm intervals each. Green puncta (yellow arrows) represent
929 autophagosomes. White arrows in (E(d, f)) and F(b) mark phagosomes in which mNG signal was
930 detected, indicating the existence of autophagosomes/phagosome fusion events. Scale bars are 5 µm.
931

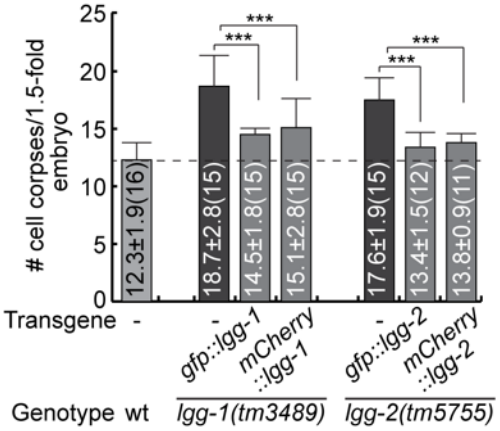

932
933
934 **Figure S5. The expression of *lgg-1* and *lgg-2* cDNA in engulfing cells suppresses the Ced**
935 **phenotype of *lgg-1* and *lgg-2* null mutants, respectively.**
936 GFP- and mCherry-tagged reporters for LGG-1 and LGG-2 are expressed in engulfing cells
937 under the control of the P_{ced-1} promoter in *lgg-1(tm3489)* and *lgg-2(tm5755)* mutant embryos,
938 respectively. The bar graph displays the average number of somatic cell corpses in *lgg-1(tm3489)* and
939 *lgg-2(tm5755)* mutant embryos at the 1.5-fold stage, both with and without the expression of the
940 rescuing construct. The number of embryos scored for each strain is in parentheses. Bars represent
941 the mean, and the error bars indicate standard deviation. Brackets above the bars indicate the
942 samples that are compared by the Student *t*-test. *p*-values are summarized as such: *, 0.001 < p <
943 0.05; **, 0.0001 < p <0.001; ***, p <0.0001; ns, no significant difference.
944

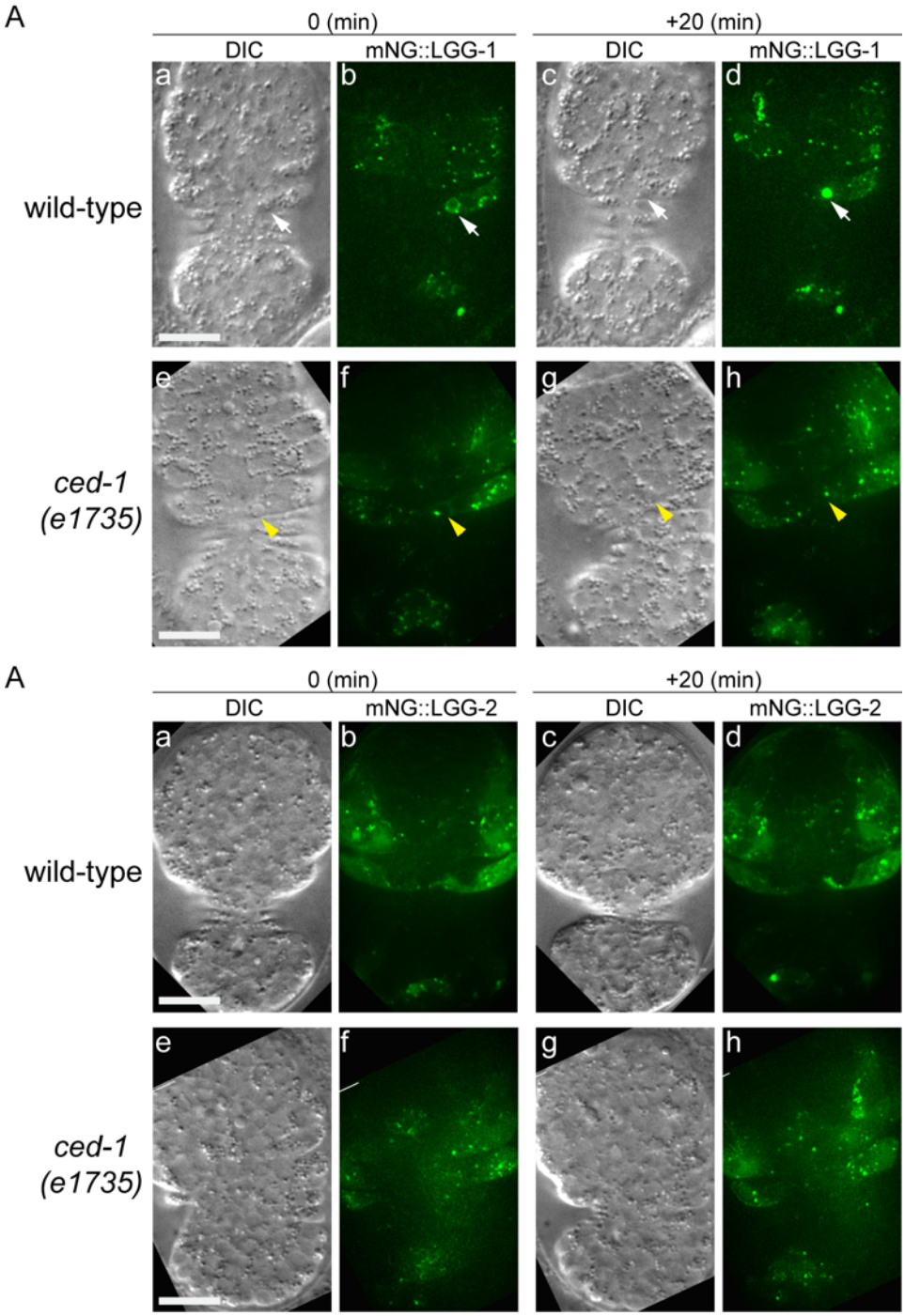

Figure S6. The generation of autophagosomes is normal in *ced-1* mutants.

Images of wild-type and *ced-1(e1735)* mutant embryos expressing P_{ced-1} *mNG::lgg-1* (A) or P_{ced-1}*lgg-2::mNG* (B) are presented. (a-b and e-f) Embryos are at ~370 min post-1st cleavage; (c-d and g-h) Embryos 20 min later. (a, c, e, g) DIC images. (b, d, f, h) 2-D projection of 14 consecutive Z-sections at 0.5 µm interval each. Green puncta represent autophagosomes. White arrows in (A(a-d)) marks one C3 phagosome, onto which LGG-1::mNG puncta are recruited in (a-b); 20 min later (c-d), LGG-1::mNG enters this phagosome, showing an autophagosomes/phagosome fusion event. Yellow

954 arrowheads in (A(e-h)) marks one C3 phagosome on the surface, of which only one mNG punctum was
955 found (f), and no mNG signal enters the phagosome (h), indicating the lack of recruitment and fusion.
956 Scale bars are 10 μm.
957
958 **Table S1.**
959

Reagent Type	Designation	Source or Reference	Additional information
E. coli	OP50	CGC	OP50
C. elegans	N2	CGC	Wild-type Bristol N2
C elegans	ZH0989	[19]	*unc-76(e911) V enIs36 [pUNC-76(+)(20ng/ul), pZZ610(Pced-1 ced-1::gfp) (5ng/ml),pIH1(Pced-1 2xFYVE::mRFP)(5ng/ul)] V*
C. elegans	ZH2573	This study	*lgg-2(tm5755) IV ; unc-76(e911) V ; enEx1223 [pXL89(Pced-1mcherry::lgg-2, 10ng/ul) + pUNC-76(25ng/ul)]*
C. elegans	ZH2632	This study	*lgg-2(tm5755) IV ; unc-76(e911) V ; enEx1267 [Punc-76(+) 20ng/ul, pTY02(Pced-1::gfp::lgg2)5ng/ul]*
C. elegans	ZH2715	This study	*rab-7 (ok511) II / mIn1 II ; unc-76(e911) V ; enEx1320 I [pUNC-76(+)(20ng/ul), pXL89(Pced-1mCherry::lgg-2)(5ng/ul)]*
C. elegans	ZH2782	This study	*rab-7 (ok511) II / mIn1 II ; unc-76(e911) V ; enEx1376 [pUNC-76(+)(20ng/ul), pZZ1091(Pced-1 mCherry::lgg-1) (5ng/ul)]*
C. elegans	ZH2831	This study	*lgg-1(tm3489) II / mIn1 II ; lgg-2(tm5755) IV*
C. elegans	ZH2835	This study	*lgg-1(tm3489) II / mIn1 II ; unc-76(e911) V enIs36 [pUNC-76(+)(20ng/ul), pZZ610(Pced-1 ced-1::gfp) (5ng/ul),pIH1(Pced-1 2xFYVE::mRFP)(5ng/ul)] V*
C. elegans	ZH2838	This study	*lgg-1(tm3489) II / mIn1 II ; unc-76(e911) V ; enEx1428 [pUNC-76(+)(20ng/ul), pZZ1052(Pced-1 gfp::lgg-1) (5ng/ul))]*
C. elegans	ZH2841	This study	*lgg-1(tm3489) II / mIn1 II ; unc-76(e911) V ; enEx1431 [pUNC-76(+)(20ng/ul), pZZ1091(Pced-1 mCherry ::lgg-1) (5ng/ul))]*
C. elegans	ZH2875	This study	*lgg-2(tm5755) IV ; unc-76(e911) V enIs36 [pUNC-76(+)(20ng/ul), pZZ610(Pced-1 ced-1::gfp) (5ng/ml),pIH1(Pced-1 2xFYVE::mRFP)(5ng/ul)] V*
C. elegans	ZH2889	This study	*unc-76(e911) V ; enEx1459 [pUNC-76 20ng/ul, pNL9(Pced-1 PH::mrfp) (5ng/ul),(pOPR004)Pced-1 mNG::lgg-2 5ng/ul)]*
C. elegans	ZH2903	This study	*atg-9(bp564) V him-5(e1490) V ; lin-15AB(n765ts) X ; enEx1468 [Plin-15(+) 50ng/ul, pNL9(Pced-1 PH::mrfp) (5ng/ul), pOPR007(Pced-1 mNG::lgg-1) (5ng/ul)]*
C. elegans	ZH2907	This study	*vps-18(tm1125) II ; unc-76(e911) V ; enIs80 [pUNC-76(+)(20ng/ul), pZZ985(Pced-1 ced-1::gfp) (5ng/ml),pZZ1091(Pced-1mCherry::lgg-1)(5ng/ul)] IV*
C. elegans	ZH2916	This study	*ced-1(e1735) I ; unc-76(e911) V ; enEx1470 [pOPR007(Pced-1 mNG::lgg-1) (5ng/ul) + pUNC-76(+) (20ng/ul) + pNL9(Pced-1 PH::mrfp) (5ng/ul)]*

C. elegans	ZH2918	This study	*unc-76(e911) V ; enIs80 [pUNC-76(+)(20ng/ul), pZZ985(P_{ced-1} ced-1::gfp) (5ng/ml),pZZ1091(Pced-1mCherry::lgg-1)(5ng/ul)]IV*
C. elegans	ZH2919	This study	*enIs82 [pUNC-76(+)(20ng/ul), pZZ985(Pced-1 ced-1::gfp) (5ng/ml),pZZ1091(Pced-1mCherry::lgg-1)(5ng/ul)] II ; unc-76(e911) V*
C. elegans	ZH2921	This study	*enIs85[pUNC-76(+)(20ng/ul), pNL9(Pced-1 PH::mrfp) (5ng/ml),pOPR004(Pced-1mNG::lgg-2)(5ng/ul)] V unc-76(e911) V.*
C. elegans	ZH2922	This study	*atg-9(bp564) V him-5(e1490) V ; lin-15AB(n765ts) X ; enEx1472 [Plin-15(+) 50ng/ul, pNL9(Pced-1 PH::mrfp) (10ng/ul), (pOPR004) Pced-1 mNG::lgg-2 10ng/ul]*
C. elegans	ZH2929	This study	*vps-18(tm1125) II ; unc-76(e911) V ; enIs83 [pUNC-76(+)(20ng/ul), pZZ985(Pced-1 ced-1::gfp) (5ng/ml),pXL89(Pced-1mCherry::lgg-2)(5ng/ul)] X*
C. elegans	ZH2934	This study	*ced-1(e1735) I ; unc-76(e911) V enIs85 [pUNC-76(+)(20ng/ul), pNL9(Pced-1 PH::mrfp) (5ng/ul),pOPR004(Pced-1mNG::lgg-2)(5ng/ul)] V*
C. elegans	ZH2950	This study	*enIs82 [pUNC-76(+)(20ng/ul), pZZ985($Pced_{-1}$ ced-1::gfp) (5ng/ml),pZZ1091(Pced-1mCherry::lgg-1)(5ng/ul)] II ; atg-7(bp411) IV ; unc-76(e911) V*
C. elegans	ZH2951	This study	*atg-7(bp411) IV ; enIs83 [pUNC-76(+)(20ng/ul), pZZ985(Pced-1 ced-1::gfp) (5ng/ml),pXL89(Pced-1mCherry::lgg-2)(5ng/ul)] X*
C. elegans	ZH2952	This study	*enIs82 [pUNC-76(+)(20ng/ul), pZZ985(Pced-1 ced-1::gfp) (5ng/ml),pZZ1091(Pced-1mCherry::lgg-1)(5ng/ul)] II ; atg-13(bp414) III*
C. elegans	ZH2953	This study	*atg-13(bp414) III ; enIs83 [pUNC-76(+)(20ng/ul), pZZ985(Pced-1 ced-1::gfp) (5ng/ml),pXL89(Pced-1mCherry::lgg-2)(5ng/ul)] X*
C. elegans	ZH2954	This study	*epg-8(bp251) I ; enIs82 [pUNC-76(+)(20ng/ul), pZZ985(Pced-1 ced-1::gfp) (5ng/ul),pZZ1091(Pced-1mCherry::lgg-1)(5ng/ul)] II ; unc-76(e911) V*
C. elegans	ZH2955	This study	*epg-8(bp251) I ; unc-76(e911) him-5(1490) V ; enIs83 [pUNC-76(+)(20ng/ul), pZZ985(Pced-1 ced-1::gfp) (5ng/ul),pXL89(Pced-1mCherry::lgg-2)(5ng/ul)] X*
C. elegans	ZH2980	This study	*atg-7(bp411) IV ; enIs36 [pUNC-76(+)(20ng/ul), pZZ610(Pced-1 ced-1::gfp) (5ng/ml),pIH1(Pced-1 2xFYVE::mRFP)(5ng/ul)] V unc-76(e911) V*
C. elegans	ZH2992	This study	*enIs87 [pUNC-76 20ng/ul, pNL9(Pced-1 PH::mrfp) (5ng/ul), pOPR007(Pced-1 mNG::lgg-1) (5ng/ul)]I ; unc-76(e911) V*
C. elegans	ZH2994	This study	*enIs82 [pUNC-76(+)(20ng/ul), pZZ985(Pced-1 ced-1::gfp) (5ng/ml),pZZ1091(Pced-1mCherry::lgg-1)(5ng/ul)] II ; ced-6(n2095) III ; unc-76(e911) V*
C. elegans	ZH2995	This study	*ced-6(n2095) III ; unc-76(e911) V ; enIs83 [pUNC-76(+)(20ng/ul), pZZ985(Pced-1 ced-1::gfp) (5ng/ml),pXL89(Pced-1mCherry::lgg-2)(5ng/ul)] X*
C. elegans	ZH3009	This study	*ced-5(n1812) IV ; unc-76(e911) V ; enIs83 [pUNC-76(+)(20ng/ul), pZZ985(Pced-1 ced-1::gfp) (5ng/ml),pXL89(Pced-1mCherry::lgg-2)(5ng/ul)] X*
C. elegans	ZH3010	This study	*enIs82 II ; ced-5(n1812) IV ; unc-76(e911) V*

C. elegans	ZH3011	This study	*enIs82 II ; ced-10(n1993) IV ; unc-76(e911) V*
C. elegans	ZH3012	This study	*ced-10(n1993) IV ; unc-76(e911) V ; enIs83 [pUNC-76(+)(20ng/ul), pZZ985(Pced-1 ced-1::gfp) (5ng/ml),pXL89(Pced-1mCherry::lgg-2)(5ng/ul)] X*
C. elegans	ZH3014	This study	*enIs87 I ; unc-76(e911) V ; dyn-1(n4039) X ; enEx21[Pdyn-1 dyn-1 8ng/ul)]*
C. elegans	ZH3015	This study	*enIs85 V unc-76(e911) V ; dyn-1(n4039) X ; enEx21[Pdyn-1 dyn-1 8ng/ul)]*

Supplemental movie legends

Movie S1. mCherry::LGG-1-labeled vesicles are recruited to the surface of a phagosome and subsequently fuse to the phagosome

Related to **Fig 1E**. This movie shows time-lapse recording images of a C3 phagosome (white arrowheads) in a wild-type embryo, starting at ~330 min post-1st cleavage. CED-1::GFP labels pseudopods, allowing the visualization of the phagosome formation process. “0 min” is the moment when pseudopods just seals. Yellow arrowheads indicate the mCherry::LGG-1^{+} puncta, and open white arrows point to the phagosome lumen containing the mCherry signal.

Movie S2. mCherry::LGG-2-labeled vesicles are recruited to the surface of a phagosome and subsequently fuse to the phagosome

Related to **Fig 1H**. This movie shows time-lapse recording images of a C3 phagosome (white arrowheads) in a wild-type embryo, starting at ~330 min post-1st cleavage. CED-1::GFP labels pseudopods, allowing the visualization of the phagosome formation process. “0 min” is the moment when pseudopods just seals. Yellow arrowheads indicate the mCherry::LGG-2^{+} puncta, and open white arrows point to the phagosome lumen containing the mCherry signal.

Movie S3. mNG::LGG-1-labeled vesicles are recruited to the surface of a phagosome and subsequently fuse to the phagosome.

Related to **Fig 1F**. This movie shows time-lapse recording images of a C3 phagosome in a wild-type embryo, starting at ~330 min post-1st cleavage. PH(hPLCγ)::mRFP labels pseudopods, allowing the visualization of the phagosome formation process. “0 min” is the moment when pseudopods just seals. Yellow arrowheads indicate mNG::LGG-1^{+} puncta, and open white arrows point to the phagosome with mNG signal in its lumen.

Movie S4. In *rab-7 (ok511),* mCherry::LGG-1-labeled vesicles fail to fuse with phagosomes.

Related to **Fig 7E**. This movie shows time-lapse recording images of a C3 phagosome in a *rab-7(ok511)* m^{-}z^{-} homozygous embryo, starting at ~330 min post-1st cleavage. “0 min” is the moment when

990 a nascent phagosome is just formed. White arrowheads mark the phagosome. Yellow arrows mark
991 mCherry::LGG-1^{+} puncta.
992
993 **Movie S5. In *rab-7(ok511)* mutants, mCherry::LGG-2-labeled vesicles fail to fuse with**
994 **phagosomes.**
995 Related to **Fig 7F**. This movie shows time-lapse recording images of a C3 phagosome in a *rab-*
996 *7(ok511)* m^{-}z^{-} homozygous embryos, starting at ~330 min post-1st cleavage. "0 min" is the moment
997 when a nascent phagosome is just formed. White arrowheads mark the phagosome. Yellow arrows
998 mark mCherry::LGG-2^{+} puncta.
999
1000 **Movie S6. In *ced-1(e1735)* mutants, mNG::LGG-1-labeled vesicles fail to be recruited to the**
1001 **phagosomal surface.**
1002 Related to **Fig 8A**. This movie shows time-lapse recording images of a C3 phagosome in a *ced-*
1003 *1(e1735)* embryo, starting at ~300 min post-1st cleavage. "0 min" is the moment when a nascent
1004 phagosome is just formed. White arrowheads mark the phagosome; yellow arrows label mNG::LGG-1^{+}
1005 puncta.
1006

1007 References

1008 1. Reddien PW, Horvitz HR (2004) The engulfment process of programmed cell death in caenorhabditis
1009 elegans. Annu Rev Cell Dev Biol 20: 193-221.
1010 2. Nagata S (2018) Apoptosis and Clearance of Apoptotic Cells. Annu Rev Immunol.
1011 3. Levin R, Grinstein S, Canton J (2016) The life cycle of phagosomes: formation, maturation, and
1012 resolution. Immunol Rev 273: 156-179.
1013 4. Schaaf MB, Keulers TG, Vooijs MA, Rouschop KM (2016) LC3/GABARAP family proteins:
1014 autophagy-(un)related functions. FASEB J 30: 3961-3978.
1015 5. Sanjuan MA, Dillon CP, Tait SW, Moshiach S, Dorsey F, et al. (2007) Toll-like receptor signalling in
1016 macrophages links the autophagy pathway to phagocytosis. Nature 450: 1253-1257.
1017 6. Green DR, Oguin TH, Martinez J (2016) The clearance of dying cells: table for two. Cell Death Differ
1018 23: 915-926.
1019 7. Martinez J, Almendinger J, Oberst A, Ness R, Dillon CP, et al. (2011) Microtubule-associated protein
1020 1 light chain 3 alpha (LC3)-associated phagocytosis is required for the efficient clearance of dead
1021 cells. Proc Natl Acad Sci U S A 108: 17396-17401.
1022 8. Martinez J, Cunha LD, Park S, Yang M, Lu Q, et al. (2016) Noncanonical autophagy inhibits the
1023 autoinflammatory, lupus-like response to dying cells. Nature 533: 115-119.
1024 9. Morishita H, Mizushima N (2019) Diverse Cellular Roles of Autophagy. Annu Rev Cell Dev Biol 35:
1025 453-475.
1026 10. Nakatogawa H (2020) Mechanisms governing autophagosome biogenesis. Nat Rev Mol Cell Biol
1027 21: 439-458.
1028 11. Cheng S, Wu Y, Lu Q, Yan J, Zhang H, et al. (2013) Autophagy genes coordinate with the class II
1029 PI/PtdIns 3-kinase PIKI-1 to regulate apoptotic cell clearance in C. elegans. Autophagy 9: 2022-
1030 2032.
1031 12. Huang S, Jia K, Wang Y, Zhou Z, Levine B (2013) Autophagy genes function in apoptotic cell
1032 corpse clearance during C. elegans embryonic development. Autophagy 9: 138-149.
1033 13. Li W, Zou W, Yang Y, Chai Y, Chen B, et al. (2012) Autophagy genes function sequentially to
1034 promote apoptotic cell corpse degradation in the engulfing cell. J Cell Biol 197: 27-35.
1035 14. Martinez J, Malireddi RK, Lu Q, Cunha LD, Pelletier S, et al. (2015) Molecular characterization of
1036 LC3-associated phagocytosis reveals distinct roles for Rubicon, NOX2 and autophagy proteins.
1037 Nat Cell Biol 17: 893-906.

1038 15. Sulston JE, Horvitz HR (1977) Post-embryonic cell lineages of the nematode, Caenorhabditis
1039 elegans. Dev Biol 56: 110-156.
1040 16. Sulston JE, Albertson DG, Thomson JN (1980) The Caenorhabditis elegans male: postembryonic
1041 development of nongonadal structures. Dev Biol 78: 542-576.
1042 17. Ellis RE, Jacobson DM, Horvitz HR (1991a) Genes required for the engulfment of cell corpses
1043 during programmed cell death in Caenorhabditis elegans. Genetics 129: 79-94.
1044 18. Mangahas PM, Zhou Z (2005) Clearance of apoptotic cells in Caenorhabditis elegans. Semin Cell
1045 Dev Biol 16: 295-306.
1046 19. Yu X, Lu N, Zhou Z (2008) Phagocytic receptor CED-1 initiates a signaling pathway for degrading
1047 engulfed apoptotic cells. PLoS Biol 6: e61.
1048 20. Zhou Z, Hartwieg E, Horvitz HR (2001b) CED-1 is a transmembrane receptor that mediates cell
1049 corpse engulfment in C. elegans. Cell 104: 43-56.
1050 21. Yu X, Odera S, Chuang CH, Lu N, Zhou Z (2006) C. elegans Dynamin mediates the signaling of
1051 phagocytic receptor CED-1 for the engulfment and degradation of apoptotic cells. Dev Cell 10:
1052 743-757.
1053 22. Shen Q, He B, Lu N, Conradt B, Grant BD, et al. (2013) Phagocytic receptor signaling regulates
1054 clathrin and epsin-mediated cytoskeletal remodeling during apoptotic cell engulfment in C.
1055 elegans. Development 140: 3230-3243.
1056 23. Lu N, Shen Q, Mahoney TR, Neukomm LJ, Wang Y, et al. (2012) Two PI 3-kinases and one PI 3-
1057 phosphatase together establish the cyclic waves of phagosomal PtdIns(3)P critical for the
1058 degradation of apoptotic cells. PLoS Biol 10: e1001245.
1059 24. Lu N, Shen Q, Mahoney TR, Liu X, Zhou Z (2011) Three sorting nexins drive the degradation of
1060 apoptotic cells in response to PtdIns(3)P signaling. Mol Biol Cell 22: 354-374.
1061 25. Lu N, Zhou Z (2012) Membrane trafficking and phagosome maturation during the clearance of
1062 apoptotic cells. Int Rev Cell Mol Biol 293: 269-309.
1063 26. Manil-Segalen M, Lefebvre C, Jenzer C, Trichet M, Boulogne C, et al. (2014) The C. elegans LC3
1064 acts downstream of GABARAP to degrade autophagosomes by interacting with the HOPS
1065 subunit VPS39. Dev Cell 28: 43-55.
1066 27. Lu N, Yu X, He X, Zhou Z (2009) Detecting apoptotic cells and monitoring their clearance in the
1067 nematode Caenorhabditis elegans. Methods Mol Biol 559: 357-370.

1068 28. Wu F, Watanabe Y, Guo XY, Qi X, Wang P, et al. (2015) Structural Basis of the Differential
1069 Function of the Two C. elegans Atg8 Homologs, LGG-1 and LGG-2, in Autophagy. Mol Cell
1070 60: 914-929.
1071 29. Tsien RY (1998) The green fluorescent protein. Annu Rev Biochem 67: 509-544.
1072 30. Shaner NC, Campbell RE, Steinbach PA, Giepmans BN, Palmer AE, et al. (2004) Improved
1073 monomeric red, orange and yellow fluorescent proteins derived from Discosoma sp. red
1074 fluorescent protein. Nat Biotechnol 22: 1567-1572.
1075 31. Shinoda H, Ma Y, Nakashima R, Sakurai K, Matsuda T, et al. (2018) Acid-Tolerant Monomeric
1076 GFP from Olindias formosa. Cell Chem Biol 25: 330-338 e337.
1077 32. Tian Y, Li Z, Hu W, Ren H, Tian E, et al. (2010) C. elegans screen identifies autophagy genes
1078 specific to multicellular organisms. Cell 141: 1042-1055.
1079 33. Yang P, Zhang H (2011) The coiled-coil domain protein EPG-8 plays an essential role in the
1080 autophagy pathway in C. elegans. Autophagy 7: 159-165.
1081 34. Zhang H, Baehrecke EH (2015) Eaten alive: novel insights into autophagy from multicellular model
1082 systems. Trends Cell Biol.
1083 35. Gomes LC, Odedra D, Dikic I, Pohl C (2016) Autophagy and modular restructuring of metabolism
1084 control germline tumor differentiation and proliferation in C. elegans. Autophagy 12: 529-546.
1085 36. Lin L, Yang P, Huang X, Zhang H, Lu Q, et al. (2013) The scaffold protein EPG-7 links cargo-
1086 receptor complexes with the autophagic assembly machinery. J Cell Biol 201: 113-129.
1087 37. Lu Q, Yang P, Huang X, Hu W, Guo B, et al. (2011) The WD40 repeat PtdIns(3)P-binding protein
1088 EPG-6 regulates progression of omegasomes to autophagosomes. Dev Cell 21: 343-357.
1089 38. Wu F, Wang P, Shen Y, Noda NN, Zhang H (2016) Small differences make a big impact: Structural
1090 insights into the differential function of the 2 Atg8 homologs in C. elegans. Autophagy 12: 606-
1091 607.
1092 39. Balderhaar HJ, Ungermann C (2013) CORVET and HOPS tethering complexes - coordinators of
1093 endosome and lysosome fusion. J Cell Sci 126: 1307-1316.
1094 40. Szatmari Z, Sass M (2014) The autophagic roles of Rab small GTPases and their upstream
1095 regulators: a review. Autophagy 10: 1154-1166.
1096 41. McEwan DG, Popovic D, Gubas A, Terawaki S, Suzuki H, et al. (2015) PLEKHM1 regulates
1097 autophagosome-lysosome fusion through HOPS complex and LC3/GABARAP proteins. Mol
1098 Cell 57: 39-54.

1099 42. Xiao H, Chen D, Fang Z, Xu J, Sun X, et al. (2009) Lysosome biogenesis mediated by vps-18 affects
1100 apoptotic cell degradation in Caenorhabditis elegans. Mol Biol Cell 20: 21-32.
1101 43. Wu YC, Stanfield GM, Horvitz HR (2000) NUC-1, a caenorhabditis elegans DNase II homolog,
1102 functions in an intermediate step of DNA degradation during apoptosis. Genes Dev 14: 536-548.
1103 44. Guo P, Hu T, Zhang J, Jiang S, Wang X (2010) Sequential action of Caenorhabditis elegans Rab
1104 GTPases regulates phagolysosome formation during apoptotic cell degradation. Proc Natl Acad
1105 Sci U S A 107: 18016-18021.
1106 45. Qu X, Zou Z, Sun Q, Luby-Phelps K, Cheng P, et al. (2007) Autophagy gene-dependent clearance of
1107 apoptotic cells during embryonic development. Cell 128: 931-946.
1108 46. Jenzer C, Simionato E, Largeau C, Scarcelli V, Lefebvre C, et al. (2019) Autophagy mediates
1109 phosphatidylserine exposure and phagosome degradation during apoptosis through specific
1110 functions of GABARAP/LGG-1 and LC3/LGG-2. Autophagy 15: 228-241.
1111 47. Fazeli G, Stetter M, Lisack JN, Wehman AM (2018) C. elegans Blastomeres Clear the Corpse of the
1112 Second Polar Body by LC3-Associated Phagocytosis. Cell Rep 23: 2070-2082.
1113 48. Fazeli G, Trinkwalder M, Irmisch L, Wehman AM (2016) C. elegans midbodies are released,
1114 phagocytosed and undergo LC3-dependent degradation independent of macroautophagy. J Cell
1115 Sci 129: 3721-3731.
1116 49. Vieira OV, Botelho RJ, Grinstein S (2002) Phagosome maturation: aging gracefully. Biochem J 366:
1117 689-704.
1118 50. Spang A (2016) Membrane Tethering Complexes in the Endosomal System. Front Cell Dev Biol 4:
1119 35.
1120 51. Kinchen JM, Doukoumetzidis K, Almendinger J, Stergiou L, Tosello-Trampont A, et al. (2008) A
1121 pathway for phagosome maturation during engulfment of apoptotic cells. Nat Cell Biol 10: 556-
1122 566.
1123 52. Jiang P, Nishimura T, Sakamaki Y, Itakura E, Hatta T, et al. (2014) The HOPS complex mediates
1124 autophagosome-lysosome fusion through interaction with syntaxin 17. Mol Biol Cell 25: 1327-
1125 1337.
1126 53. Takáts S, Pircs K, Nagy P, Varga Á, Kárpáti M, et al. (2014) Interaction of the HOPS complex with
1127 Syntaxin 17 mediates autophagosome clearance in Drosophila. Mol Biol Cell 25: 1338-1354.
1128 54. Stroupe C, Collins KM, Fratti RA, Wickner W (2006) Purification of active HOPS complex reveals
1129 its affinities for phosphoinositides and the SNARE Vam7p. EMBO J 25: 1579-1589.

1130 55. Jeschke A, Haas A (2018) Sequential actions of phosphatidylinositol phosphates regulate
1131 phagosome-lysosome fusion. Mol Biol Cell 29: 452-465.
1132 56. Wood WB, Researchers tCo*Ce* (1988) The Nematode *Caenorhabditis elegans*. Cold Spring Harbor,
1133 NY: Cold Spring Harbor Laboratory.
1134 57. Riddle DL, Blumenthal T, Meyer BJ, Priess JR, editors (1997) C. elegans II. Plainview, NY: Cold
1135 Spring harbor Laboratory Press.
1136 58. Edgley ML, Baillie DL, Riddle DL, Rose AM (2006) Genetic balancers. WormBook: 1-32.
1137 59. Bloom L, Horvitz HR (1997) The Caenorhabditis elegans gene unc-76 and its human homologs
1138 define a new gene family involved in axonal outgrowth and fasciculation. Proc Natl Acad Sci U
1139 S A 94: 3414-3419.
1140 60. Jin Y (1999) Transformation. In: Hope IA, editor. C elegans, a practical approach. Oxford: Oxford
1141 University Press. pp. 69-96.
1142 61. Haley R, Wang Y, Zhou Z (2018) The small GTPase RAB-35 defines a third pathway that is
1143 required for the recognition and degradation of apoptotic cells. PLoS Genet 14: e1007558.
1144 62. Shaner NC, Lambert GG, Chammas A, Ni Y, Cranfill PJ, et al. (2013) A bright monomeric green
1145 fluorescent protein derived from Branchiostoma lanceolatum. Nat Methods 10: 407-409.
1146
1147